ANALYSIS OF ALTERNATIVE FUEL COMBUSTION IN A PERFECTLY STIRRED REACTOR

A Thesis

Presented in Partial Fulfillment of the Requirements for

Graduation with Distinction in the

Department of Mechanical Engineering at

The Ohio State University

By

A. Tyler Little

* * * * *

The Ohio State University

February 2007

ABSTRACT

The combustion of methane, isooctane, and ethanol with air has been simulated in a perfectly stirred reactor. The CHEMKIN computer code was used to facilitate the solution of the chemical kinetic mechanisms obtained from literature. The models used for methane, isooctane, and ethanol were developed by Miller and Bowman, Maurice *et al*., and Marinov, respectively. The reaction mechanisms of methane and isooctane include comprehensive submechanisms describing NO_x chemistry, whereas that for ethanol describes only C/H/O interaction. The objective of this work is to examine the effects of reactor pressure and charge residence time on adiabatic flame temperatures and emissions over a wide range of equivalence ratios. For methane and isooctane, the production of pollutants carbon monoxide (CO) and nitric oxide (NO) is investigated, while for ethanol only CO formation is considered. A comparison of fuels is also conducted to assess their relative merit. Here, the emissions of CO_2 and H_2O have also been included because of their contribution to greenhouse gases.

Flame temperatures have been discovered to increase with reactor pressure and residence time, and it was revealed that isooctane generates the highest temperatures regardless of inlet mixture strength. With an increase in pressure, CO formation decreases for each fuel, while the amount of NO produced increases only for methane. The effect of pressure on NO formation for isooctane combustion depends on the fuel-air stoichiometry. As residence time is increased, lower CO and higher NO are produced by each fuel. The strong dependence on temperature for NO formation is also demonstrated. It is discovered that the production of NO is reduced when

residence times are sufficiently short due to the relatively slow reaction rates of the mechanism primarily responsible for high temperature formation. The fuel emissions comparison reveals that, in general, CO and CO_2 production is largest for isooctane and ethanol, which yield similar values. It is also observed that NO formation is substantially higher for isooctane than methane, while isooctane combustion generates less H_2O than the comparable levels for methane and ethanol.

ACKNOWLEDGMENTS

I would like to thank my advisor, Dr. Ahmet Selamet, for the opportunity to conduct undergraduate research and for the guidance and support he has provided over the course of this project. His feedback has been instrumental to my understanding of the subject matter. Additionally, his input and attention to detail on the writing of this thesis is very much appreciated. I also wish to express sincere gratitude to Cam Giang for the discussions of results and to Dr. Iljae Lee for his help with the formatting of this report.

TABLE OF CONTENTS

LIST OF TABLES

LIST OF FIGURES

NOMENCLATURE

A	Pre-exponential factor
A/F	Air/Fuel ratio
b	Temperature exponent
c_p	Specific heat at constant pressure
Da	Damkohler number
E_A	Activation energy
h	Specific enthalpy
k	Reaction rate constant
LHV	Lower heating value
M	Molecular weight
m	Mass
$\dot{m}$	Mass flow rate
N	Total number of species
p	Reactor pressure
ppm	Parts per million
PSR	Perfectly stirred reactor
Q	Heat input/output
$\dot{Q}_{loss}$	Rate of heat loss

$\overline{R}$	Universal gas constant
RON	Research octane number
MON	Motor octane number
T	Temperature
V	Reactor volume
X	Mass fraction
y	Mole fraction

Greek Symbols

Δ	Quantity change
ρ	Density of fuel-air mixture
τ	Residence time
ϕ	Fuel/Air equivalence ratio
$\dot{\omega}$	Molar production rate of species per unit volume

Subscripts

f	Fuel
in	Inlet
out	Outlet
S	Species S

Superscripts

i	Inlet
o	Outlet

CHAPTER 1

INTRODUCTION

The internal combustion engine has long depended on a limited number of fuels for operation. The majority of spark ignition engines are gasoline powered, whereas the compression ignition engine is dominated by diesel fuel combustion. Advancements in efficiencies of these engines have been the focus of research efforts for many years. As concerns for the environment have increased recently, much attention has also been given to the reduction of emissions that are detrimental to the atmosphere. Strict emission regulations are being passed which force researchers to seek ways to minimize the production of harmful pollutants while maintaining the efficiency improvements that have been and continue to be made. In addition, high oil prices and the emergence of renewable fuels, such as ethanol, have driven many scientists to investigate alternative sources of propulsion for the automobile. The term "alternative fuel" has come to be regarded as a viable solution to the challenges outlined here. Knowledge of the combustion performance of these fuels is vital if their use is to become widespread in energy conversion devices.

The study of chemical kinetics of reacting systems offers a means of predicting the species composition and gas temperature of the products of combustion. Significant effort has been devoted to developing complex kinetic models of a number of fuels to produce accurate

results over a wide range of operating conditions and reactor configurations. A perfectly stirred reactor (PSR) model is often used to test kinetic mechanisms during development. The advantage of such a model is that the rate of conversion of reactants to products is controlled by the chemical reaction rates rather than the mixing of the fuel and oxidizer molecules. Assuming mixing has been successfully modeled, the use of a PSR reduces the computational demand of the mathematical model. This enables the user to investigate larger, more complex mechanisms than would otherwise be possible.

The objective of this work is to predict the emissions and product gas temperatures of three different fuel-air mixtures under various operating conditions in a perfectly stirred reactor. The fuels analyzed are methane, isooctane, and ethanol, and their kinetic mechanisms are constructed by Miller and Bowman (1989), Maurice *et al*. (1996), and Marinov (1999), respectively. The effect of varying reactor pressure and residence time for a wide range of equivalence ratios has been studied. The focus of the species composition study for methane and isooctane is on the pollutants CO and NO. The former is a dangerous toxic gas that can cause death and the latter participates in ozone layer depletion. Because the ethanol mechanism by Marinov does not include NO kinetics, only the production of CO is studied. Finally, a comparison between fuels is given to assess their relative merit. In this section, the species composition study has been extended to include the greenhouse gases CO_2 and H_2O that are formed in the combustion of hydrocarbons.

CHAPTER 2

FUNDAMENTALS OF HYDROCARBON COMBUSTION

The kinetic mechanisms used to model hydrocarbon combustion are generally composed of a large number of elementary reactions to describe a single comprehensive overall reaction in which the initial fuel and oxidizer combine to form the final products. The rates in which reactions proceed are primarily dictated by collisions of two molecules that may have the capability to react. Therefore, the most common elementary reactions used in mechanism construction are bimolecular in that two species collide and react to form two new species. To illustrate, consider an arbitrary bimolecular second order reaction

$$A + B \longrightarrow C + D\,. \tag{2.1}$$

The rate at which such a reaction proceeds is proportional to the concentration of the reactant species,

$$\frac{d[A]}{dt} = -k[A][B]\,, \tag{2.2}$$

where the notation [S] denotes the molar concentration of species S. The rate constant k is a function of temperature T and is the parameter used to describe each elementary reaction composing the entire kinetic mechanism. A reaction will only take place, however, if the colliding molecules possess an adequate amount of energy called the activation energy E_A. Kinetic theory shows that the fraction of all collisions that possess energy greater than E_A is

given by the Boltzmann factor $\exp\left(\frac{-E_A}{\overline{R}T}\right)$. Determination of reaction rates also requires that the frequency of molecular collisions be taken into account in the form of a pre-exponential factor A. The rate constant k is then typically expressed in a modified Arrhenius form as

$$k = AT^b \exp\left(\frac{-E_A}{\overline{R}T}\right), \tag{2.3}$$

where A, b, and E_A are parameters determined experimentally and $\overline{R}$ is the universal gas constant. The exponent b becomes particularly important in systems where temperatures vary widely. Mechanism construction is accomplished by including all elementary reactions believed to contribute either directly or indirectly to the formation of products. Accompanying each reaction are unique values of the parameters in Eq. (2.3).

Most combustion processes are governed by chain reactions initiated via the production of unstable radicals from the dissociation of one of the reacting species. The radicals then initiate a relatively fast chain of steps reacting with other molecules. A simple chain propagating reaction involves the production of one radical for each consumed, however, in chain branching reactions two or more radicals are generated from the consumption of one. This leads to a rapid buildup of radical concentration and hence a very fast overall reaction explosive in character. The termination of the chain occurs when the reaction of two radicals or a radical reacting with another molecule form a stable species. Termination can also be achieved with the formation of a radical with lower activity that cannot propagate the chain.

The oxidation of saturated hydrocarbons of the form C_nH_{2n+2} has been described by Fristrom and Westenberg (1965) to occur in two thermal zones. In the primary reaction zone, fuel molecules are attacked and reduced to CO, H_2, H_2O, and various radicals (H, O, OH). It is also here that other intermediates are formed. In the secondary reaction zone, oxidation of CO

and H_2 occurs. They suggest that in oxygen-rich saturated hydrocarbon flames, lower order hydrocarbons form according to

$$OH + C_nH_{2n+2} \longrightarrow H_2O + C_nH_{2n+1} \Rightarrow C_{n-1}H_{2n-2} + CH_3\,, \tag{2.4}$$

while in fuel-rich flames

$$H + C_nH_{2n+2} \longrightarrow H_2 + C_nH_{2n+1} \tag{2.5}$$

is the scheme. These characteristics have been confirmed by Dryer and Glassman (1978) via high-temperature flow reactor studies which also revealed that the fuel is consumed prior to the majority of the energy release. This evidence led Glassman (1996) to characterize the general oxidation of hydrocarbons into three steps: (1) following ignition, the primary fuel disappears with little or no energy release producing unsaturated hydrocarbons and H_2 with some hydrogen being oxidized to water; (2) the unsaturated hydrocarbons are further oxidized to CO and H_2, and essentially all hydrogen is simultaneously oxidized to water; and (3) finally, most of the heat from the overall reaction is released from the oxidization of CO to CO_2. For a more detailed discussion on hydrocarbon oxidation, including characteristics unique to methane, higher order hydrocarbons, and alcohols, the reader is referred to Glassman (1996).

CHAPTER 3

DESCRIPTION OF CHEMKIN

CHEMKIN (2006) is a computer program designed to facilitate the solution of complex chemical kinetics problems. It features a large variety of flame simulators and reactor models including the *perfectly stirred reactor* (PSR) used in the present work. The software includes an extensive library of gas-phase kinetics, surface kinetics, gas transport, and thermodynamic data. In the pre-processing stage, the user is required to create a chemistry set that specifies applicable data. It is here that the kinetic mechanism with each elementary reaction and associated parameters A, b, and E_A are loaded into a gas-phase kinetics file. The thermodynamic data file can then be loaded from the internal library. Complicated mechanisms with many different species may require external thermodynamic data not supplied by CHEMKIN. A FORTRAN computer programming language is then used to communicate modeling conditions and reactor parameters. Once the model set-up is complete and the run executed, the user can open the post-processing module. Here, specific data of interest can be selected for plotting or exporting.

Governing equations for the perfectly stirred reactor are based on conservation of mass, energy, and species. This includes net generation of chemical species within the reactor volume and net loss of species and mass to surfaces in the reactor. The present work assumes no species

deposits on the reactor walls, hence the inlet and outlet mass flow rates are equal. The mass conservation of each species then takes the form

$$\dot{m}\left(X_S^o - X_S^i\right) - \dot{\omega}_S V M_S = 0, \tag{3.1}$$

where $\dot{m}$ is the total mass flow rate of the mixture, X_S^i and X_S^o are inlet and outlet mass fractions, respectively, $\dot{\omega}_S$ is the molar rate of production of species *S* per unit volume, *V* is the reactor volume, and M_S is the molecular weight of species *S*. Similarly, conservation of energy is

$$\dot{m}\sum_{S=1}^{N}\left(X_S^o h_S^o - X_S^i h_S^i\right) + \dot{Q}_{loss} = 0. \tag{3.2}$$

Here, h_S^i and h_S^o are the inlet and outlet specific enthalpies of species *S*, respectively, $\dot{Q}_{loss}$ is the reactor heat loss, and *N* is the total number of species. Residence time is defined in the current study as

$$\tau = \frac{\rho V}{\dot{m}} \tag{3.3}$$

instead of mass flow rate. The density ρ is determined from the ideal gas equation of state,

$$\rho = \frac{pM}{\overline{R}T}, \tag{3.4}$$

which introduces the pressure *p*. The conservation laws form a set of *N* + 1 nonlinear algebraic equations that account for the production of *N* species and their associated energies in Eqs. (3.1) and (3.2) as well as the temperature, which appears implicitly in terms of the enthalpy. The system of equations is solved according to the Newton algorithm method discussed in the CHEMKIN manual.

CHAPTER 4

DESCRIPTION OF MODEL

4.1 Perfectly Stirred Reactor

The combustion modeling in this study is performed through the use of a perfectly stirred reactor (PSR). PSR modeling assumes the properties within the reactor to be spatially uniform. Because the reactor contents are perfectly mixed, the system kinetics represent the limit of the Damkohler number as

$$Da = \frac{\text{Mixing Time}}{\text{Chemical Reaction Time}} \to 0. \tag{4.1}$$

This idealization indicates that the conversion of reactants to products is controlled by the rate at which the chemical reactions take place rather than the rate at which fuel and oxidizer molecules diffuse together. It is also assumed that there are no deposits on the reactor walls such that the inlet and outlet mass flow rates are equal.

A schematic of a PSR is shown in Figure 4.1. It is characterized by its volume V, pressure p, inlet temperature T_{in}, heat loss Q, and fuel/air equivalence ratio ϕ of the inlet mixture. A residence time τ is used in place of mass flow rate, which can be determined using the reactor volume. For all cases in this investigation, the heat loss is taken to be zero and therefore all processes are adiabatic.

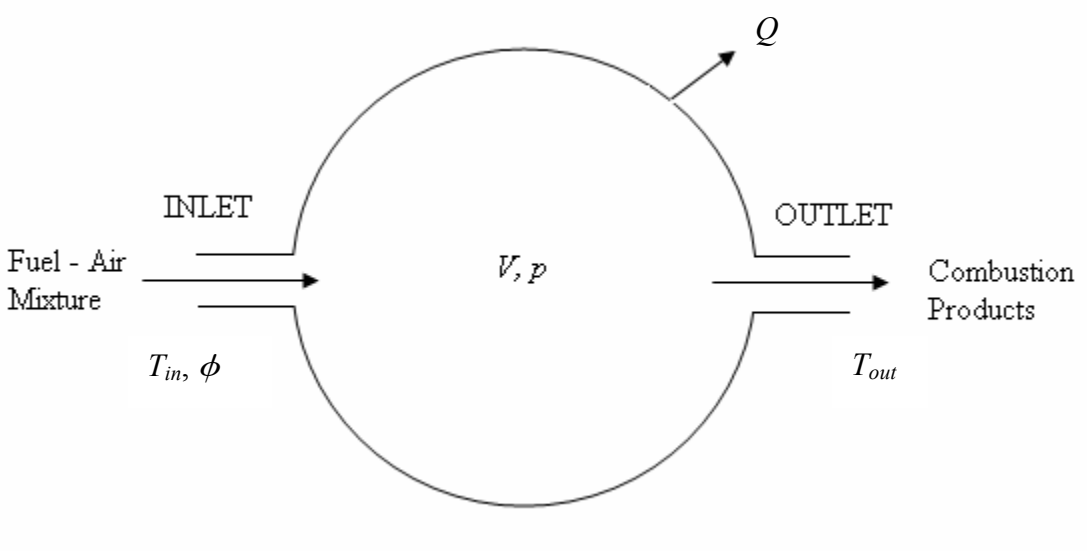

Figure 4.1: Schematic of a PSR.

4.2 Fuel and Mechanism

Three different fuels have been chosen for the present investigation: methane (CH_4), isooctane (C_8H_{18}), and ethanol (C_2H_5OH). Table 4.1, adapted from Heywood (1988), gives some basic properties of these fuels. Extensive chemical kinetic models including NO_x chemistry are used for methane and isooctane, whereas the ethanol oxidation mechanism does not include a NO_x submechanism.

Table 4.1: Selected Fuel Properties; LHV = Lower Heating Value; $(A/F)_s$ = Stoichiometric Air/Fuel Ratio; Octane Rating = (RON+MON)/2.

Fuel	Chemical Formula	Molecular Weight (kg/kmol)	LHV			$(A/F)_s$	Octane Rating
			(MJ/kg)	(MJ/kmol)	(MJ/gal)*		
Methane	CH_4	16.04	50.0	802	0.13	17.23	120
Isooctane	C_8H_{18}	114.23	44.3	5060	116.04	15.13	100
Ethanol	C_2H_5OH	46.07	26.9	1239	79.94	9.00	98

* At 20°C and 1 atm

4.2.1 Methane

The oxidation of methane is carried out according to the mechanism constructed by Miller and Bowman (1989). It contanins 53 species and 237 reversible reactions with a NO_x submechanism comprised of 86 reactions. The NO_x chemistry includes thermal and prompt NO formation as well as fuel nitrogen conversion. The model has been tested and validated against experimental data over a wide range of reactor parameters and mixture strengths for one-dimensional premixed laminar flame, perfectly stirred and plug flow reactors.

4.2.2 Isooctane

The model describing the oxidation of isooctane is that generated by Maurice *et al*. (1996). It is a complex mechanism that includes 1141 total reactions and 179 species with a NO_x submechanism consisting of 276 reactions. Thermodynamic data have been obtained from a number of sources including Himmelblau (1974), Kee *et al*. (1987), Reid *et al*. (1987), and Burcat and McBride (1993). Group additivity (Benson, 1976 and McBride, 1991) was used to generate some data not found in the databases. The experimental data to support the model is limited and thus the computational results presented here must be considered with caution.

4.2.3 Ethanol

A detailed chemical kinetic model created by Marinov (1999) is used to study the oxidation of ethanol. It contains 383 reversible reactions with 56 species. The thermodynamic data for the model was primarily taken from the CHEMKIN database (Kee *et al*., 1987) and Burcat and McBride (1993). Group additivity (Benson, 1976, Ritter and Bozzelli, 1991, and Cohen and Benson, 1993) was used for species not found in the databases. The mechanism does not include NO_x chemistry, and therefore the production of NO from the combustion of ethanol

with air is excluded from the present study. Laminar flame speed data, ignition delay data, and ethanol oxidation product profiles obtained experimentally (Marinov, 1999) support simulation results from the model.

4.3 Modeling Parameters

The dependence of the flame temperature and product species composition upon the pressure and residence time of the charge within the reactor is investigated for a range of fuel-air mixture strengths. The reactor is assumed to be a constant volume of 250 cm^3 and to be perfectly insulated such that there is no net heat transfer to or from the surroundings. The inlet stream is taken to be at 298 K for all cases with a varying ϕ of 0.6–1.4. The effect of p is examined by simulating reactor pressures of 1, 5, and 10 atm, while constraining τ to 5 ms. Similarly, the effect of varying the charge residence time is studied for τ = 1, 5, and 10 ms with a constant reactor pressure of 1 atm. A summary of the modeling conditions for each case is presented in Table 4.2.

Table 4.2: Modeling Conditions for the PSR.

Parameter Studied	Reactor Pressure (atm)	Residence Time (ms)
p	1, 5, 10	5
τ	1	1, 5, 10

CHAPTER 5

RESULTS AND DISCUSSION

5.1 Methane-Air Combustion

5.1.1 Effect of Pressure (τ = 5 ms)

5.1.1.1 Flame Temperature

The adiabatic flame temperature of methane-air combustion as a function of fuel/air equivalence ratio is shown in Figure 5.1. Temperatures increase with the reactor pressure, particularly near stoichiometric mixture strength. For each pressure considered, flame temperature reaches a maximum at an equivalence ratio of ϕ = 1.05. The temperature peaks at approximately 2082 K for 1 atm and increases by nearly 125 K for 5 atm. A smaller rise of around 29 K is seen between 5 and 10 atm for a peak value of about 2236 K. A temperature profile is also given for p = 50 atm, typical of peak in-cylinder pressures in spark ignition (SI) engines, to demonstrate the asymptotic behavior with pressure. A fivefold pressure increase to 50 atm generates approximately the same rise in temperature as doubling the pressure to 10 atm, particularly for lean and rich conditions. Only a slight increase in temperature between 5 and 10 atm can be found for the extreme stoichiometric conditions; about 5 K at the lean end of the spectrum and around 8 K at the rich end. These differences are only slightly larger for a shift

from 10 to 50 atm. The differences in lean and rich temperatures between reactor pressures of 1 and 5 atm are more significant. The model predicts increases of approximately 32 and 35 K at ϕ = 0.6 and 1.6, respectively.

An examination of the specific heat of the product mixture provides an insight into the occurrence of maximum temperatures near stoichiometric conditions. The change in temperature ΔT from the inlet mixture to the burned gas is related to the exiting mixture specific heat c_p by

$$m_f Q_{LHV} = mc_p \Delta T \,, \tag{5.1}$$

where m is the mass of the products and $m_f Q_{LHV}$ represents the fuel energy input to the reactor for complete combustion. Figure 5.2 shows the variation of the exiting mixture c_p with equivalence ratio. Specific heats were calculated from curve-fit coefficients obtained from the NIST Chemistry WebBook (2005). The curve closely resembles that of the temperature dependence on ϕ given in Figure 5.1. It is expected from Eq. (5.1) that for a given quantity of fuel, hence $m_f Q_{LHV}$, a higher ΔT would correspond to a lower mc_p. Since the temperature and specific heat dependence on ϕ are similar, the mass of the mixture must follow an opposite trend. Figure 5.3 depicts the product mc_p versus equivalence ratio for the case of p = 1 atm. The shape of the curve resembles the inverse of the temperature curve in Figure 5.1. At slightly rich conditions, mc_p attains its smallest value corresponding closely to the location of maximum temperature.

5.1.1.2 CO

The dependence of CO mole fraction, y_{CO}, on pressure is illustrated in Figure 5.4. For all pressures investigated, y_{CO} increases with equivalence ratio as expected due to the lack of oxygen in rich mixtures. Insufficient oxygen inhibits the oxidation of all of the carbon atoms into CO_2 and therefore large amounts of CO are found. Changes in pressure again have the largest effect near stoichiometric conditions. Here, the greatest amount of CO corresponds to atmospheric

pressure with a mole fraction of 0.02. This value decreases significantly at 5 atm to 0.011 and to 0.008 at 10 atm. At very lean conditions, a slightly larger amount of CO is observed for 1 atm compared to the other pressures, while the difference between 5 and 10 atm is only minute. Pressure is shown to have virtually no effect on CO concentration for the range ϕ = 1.25 – 1.35, however, the model predicts the same pressure dependency at ϕ = 1.4 as observed for the leaner conditions.

5.1.1.3 NO

The variation of NO with equivalence ratio and pressure is shown in Figure 5.5. For stoichiometric and lean conditions, the concentration of NO is observed to increase with reactor pressure. A maximum value of about 471 ppm is located at an equivalence ratio of 0.95 for 10 atm. With decreasing pressure, peak values move to higher ϕ. For 5 atm, the model predicts a maximum of nearly 406 ppm, and for 1 atm, approximately 173 ppm at equivalence ratios of 1.0 and 1.05, respectively. The peak values found near stoichiometric mixture strength demonstrate the strong dependence of NO formation on temperature as Figure 5.1 illustrates that maximum temperatures are also found in this vicinity.

The oxidation of atmospheric nitrogen is believed to be the primary source of NO formation in high temperature combustion. Termed Thermal NO, the well-known extended Zeldovich mechanism,

$$O + N_2 \rightleftarrows NO + N \tag{5.2}$$

$$N + O_2 \rightleftarrows NO + O \tag{5.3}$$

$$N + OH \rightleftarrows NO + H \tag{5.4}$$

describes this process. Turns (1996) suggests that this process is usually important only for temperatures greater than 1800 K, and since its NO formation rate is relatively slow compared to the rate of fuel oxidation, it is generally considered to be formed in post-flame gases. It can be shown (Heywood, 1988) that the initial rate of formation of NO according to this three reaction mechanism is given by

$$\frac{d[NO]}{dt} = 6\times10^{16} T^{-1/2} \exp(-69,090T^{-1})[O_2]_e^{1/2}[N_2]_e, \tag{5.5}$$

where $[S]_e$ represents the equilibrium concentration of species *S*. This expression illustrates the strong nonlinear effect of temperature on NO formation.

NO at rich conditions shows varying dependence on reactor pressure. For mixture strengths of ϕ = 1.05 and 1.1, the highest NO concentration is observed for 5 atm, followed by 10 and 1 atm. At ϕ = 1.15, NO at 1 atm surpasses that at 10 atm, and beyond this point a decrease in pressure returns a larger amount of NO.

5.1.2 Effect of Residence Time (*p* = 1atm)

5.1.2.1 Flame Temperature

The dependence of flame temperature for methane-air combustion on residence time is shown in Figure 5.6 for an equivalence ratio range of ϕ = 0.6-1.4. Peak temperatures are again located at ϕ = 1.05, with the exception of τ = 1 ms where a maximum of approximately 1983 K is attained at ϕ = 1.1-1.15. The figure depicts that flame temperatures increase with charge residence time. At τ = 5 and 10 ms, the highest temperatures are about 2082 and 2118 K, respectively. The effect of residence time is most dramatic near stoichiometric conditions. At ϕ = 1, temperature gains greater than 110 and 37 K are observed when residence time is increased from 1 to 5 and 5 to 10 ms, respectively.

5.1.2.2 CO

CO formation is shown versus fuel/air equivalence ratio for three residence times in Figure 5.7. It illustrates that a longer residence time will cause CO concentration to decrease for nearly all mixture strengths considered. The exception is at ϕ = 1.25-1.4 where y_{CO} is virtually identical for residence times of 5 and 10 ms. As discussed in section 5.1.1.2, CO increases with equivalence ratio due to inadequate oxygen needed to produce CO_2 in rich mixtures. At ϕ = 1.0, the model predicts y_{CO} = 0.026, 0.02, and 0.018 for τ = 1, 5, and 10 ms, respectively. In general, the effect of changing τ is most prominent at $\phi \leq 1.0$.

5.1.2.3 NO

The mole fraction of NO as a function of fuel/air equivalence ratio is shown in Figure 5.8 with residence time as a parameter. The plot shows that residence time plays a significant role in the formation of NO. For 5 and 10 ms, maximum values are located near stoichiometric, however, decreasing τ to 1 ms causes the peak to shift to rich conditions near ϕ = 1.3. This may suggest that the reactions comprising the extended Zeldovich mechanism, which are primarily responsible for the peaks near conditions with the highest temperatures, are too slow to have a significant impact when residence times are short. It has been suggested (Fenimore, 1971), that reactions other than the Zeldovich mechanism are responsible for significant NO formation, particularly in fuel-rich mixtures. Several studies (Hayhurst and Vance, 1983, Glarborg *et al*., 1986, Miller and Bowman, 1989, and Giang, 2002) have demonstrated that the rapid prompt NO reactions are important for such cases. The principal initiating steps for prompt NO are believed to be

$$CH + N_2 \rightleftarrows HCN + N \tag{5.6}$$

and

$$CH_2 + N_2 \rightleftarrows HCN + NH \; . \tag{5.7}$$

The HCN, N, and NH species then react with O, O_2, OH, and H to produce NO.

In general, NO mole fractions grow as charge residence time increases with the most dramatic growth near stoichiometric mixtures. Significant quantitative differences are discovered for the various residence times. The maximum values of NO are approximately 91, 173, and 275 ppm for 1, 5, and 10 ms, respectively. Levels at extremely lean conditions are negligible, and rich conditions yield about 90 ppm for τ = 5 and 10 ms at ϕ = 1.4 and drops around 36 ppm for 1 ms.

5.2 Isooctane-Air Combustion

5.2.1 Effect of Pressure (τ = 5 ms)

5.2.1.1 Flame Temperature

The adiabatic flame temperature for isooctane-air combustion versus fuel/air equivalence ratio with reactor pressure varying parametrically is shown in Figure 5.9. For p = 1 atm, temperature peaks at 2152 K at ϕ = 1.1 and decreases as the mixture becomes lean or rich of this point. Increasing the reactor pressure to 5 atm generally increases the temperature with the most significant changes at moderately lean or rich mixtures (near ϕ = 0.85 and 1.25). The temperature variance between 5 and 10 atm is small for all ϕ. Additionally, adjusting the mixture strength from about ϕ = 0.95 to 1.25 has little effect on temperature for these pressures. Maximum and minimum values for either pressure in this range are approximately 2169 and 2143 K, respectively.

5.2.1.2 CO

CO formation as a function of ϕ for the three pressures is depicted in Figure 5.10. The level of CO observed in the products increases as the inlet mixture becomes fuel-rich as discussed for the case of methane in section 5.1.1.2. The effect of changing the reactor pressure is negligible beyond $\phi = 1.25$. Shifting pressure near stoichiometric conditions results in more significant changes in y_{CO}. Specifically, a pressure increase at $\phi = 1.0$ from 1 to 5 atm will result in a decrease of y_{CO} from approximately 0.025 to about 0.012. CO differences between $p = 5$ and 10 atm are generally less; y_{CO} at 10 atm is roughly 0.009 at $\phi = 1.0$. Except for the rich conditions noted earlier, carbon monoxide levels decrease with an increase in reactor pressure.

5.2.1.3 NO

The variation of NO with equivalence ratio for $p = 1$, 5, and 10 atm is given in Figure 5.11. As pressure is decreased, the point for maximum NO becomes leaner. At 1 atm, peak NO is approximately 445 ppm at $\phi = 1.05$. Pressures of 5 and 10 atm yield maximum values of about 443 and 356 ppm at $\phi = 0.95$ and 0.9, respectively. The observation that the largest amounts of NO are located at mixtures where temperatures are high illustrates that the extended Zeldovich mechanism also plays an important role in the formation of NO in isooctane-air combustion. Peak values are similar because maximum temperatures shown in Figure 5.9 are very close for all pressures.

Trend of NO formation as a function of reactor pressure is not uniform across the mixture strength. The model predicts that for lean mixtures less than $\phi = 0.85$, NO concentration will increase accompanying a change from 1 to 5 atm and stay relatively the same when p is increased further to 10 atm. Mixtures of $\phi = 0.9$-0.95 generate largest amounts of NO for 5 atm, and for $\phi = 1.0$ and beyond, a decrease in reactor pressure results in a higher NO concentration.

5.2.2 Effect of Residence Time (p = 1 atm)

5.2.2.1 Flame Temperature

Isooctane-air adiabatic flame temperatures are given in Figure 5.12 for varying equivalence ratio and charge residence time. Temperatures peak at approximately 2052 and 2152 K for ϕ = 1.1 at τ = 1 and 5 ms, respectively. Extending the time in the reactor to 10 ms shifts the maximum temperature location to stoichiometric with a value of about 2168 K, though the variation is small for ϕ = 1.0-1.1. For all equivalence ratios considered, increasing the residence time results in a higher flame temperature. Changes are most significant between τ = 1 and 5 ms near ϕ = 1.0. Temperature differences between residence times of 5 and 10 ms are relatively uniform throughout the entire range of mixtures.

5.2.2.2 CO

Figure 5.13 depicts the effect of the residence time on CO formation for the range ϕ = 0.6-1.4. CO levels are again observed to increase with fuel/air equivalence ratio. A change in τ from 5 to 10 ms beyond ϕ = 1.2 does not have a noticeable effect on y_{CO}, and beyond ϕ = 1.3, all three residence times return very similar values. Changes are relatively uniform for lean and slightly rich mixtures up to about ϕ = 1.05, with an increase in CO accompanying longer residence times. At ϕ = 1.0, y_{CO} = 0.033, 0.025, and 0.022 for τ = 1, 5, and 10 ms, respectively.

5.2.2.3 NO

Figure 5.14 gives NO levels predicted from the model for the three residence times with equivalence ratio ranging from 0.6-1.4. The effect of residence time is significant for the majority of mixture strengths. NO peaks near stoichiometric where high temperatures exist for 5 and 10 ms at approximately 445 and 571 ppm, respectively. However, for τ = 1 ms, rich

conditions (ϕ = 1.2) yield the maximum NO of about 229 ppm. This again suggests that the extended Zeldovich mechanism responsible for high temperature NO formation may be too slow to significantly contribute to overall levels when τ = 1 ms since temperatures in Figure 5.12 exceed the 1800 K threshold for significant Thermal NO production suggested by Turns (1996) at this residence time. The prompt NO formation mechanism discussed in section 5.1.2.3 may then explain the occurrence of maximum NO in the rich regime.

NO levels at the extreme lean end of the spectrum are negligible for all residence times considered, while rich conditions at ϕ = 1.4 give approximately 210 ppm for 5 and 10 ms. In fact, little variation is observed for ϕ = 1.3-1.4 between 5 and 10 ms. Values for τ = 1 ms are only slightly lower for rich mixtures with nearly 185 ppm NO at ϕ = 1.4.

5.3 Ethanol-Air Combustion

5.3.1 Effect of Pressure (τ = 5 ms)

5.3.1.1 Flame Temperature

The adiabatic flame temperature from the ethanol-air combustion is given in Figure 5.15 over a range of ϕ = 0.6-1.4 for p = 1, 5, and 10 atm. The temperature increases with reactor pressure and peaks at slightly rich of stoichiometric. At p = 1 atm, a maximum of approximately 2078 K is achieved at ϕ = 1.1, while 5 and 10 atm generate maximum values of about 2223 and 2259 K, respectively, at ϕ = 1.05. The increase in temperature between 1 and 5 atm is more dramatic than a change from 5 to 10 atm, and the most significant differences occur near stoichiometric for both cases.

5.3.1.2 CO

Shown in Figure 5.16 is the variation of CO formation with equivalence ratio for the three reactor pressures. As is the case for methane and isooctane combustion, the largest quantities of CO exist at rich conditions where oxygen is lacking. Stoichiometric and slightly lean mixtures give way to the most significant changes in y_{CO} when pressure is adjusted. At ϕ = 1.0, y_{CO} = 0.026, 0.014, and 0.01 for p = 1, 5, and 10 atm, respectively. CO decreases as reactor pressure is increased for all mixtures except rich where changes in pressure do not have an appreciable effect. Beyond ϕ = 1.15, changes in y_{CO} are difficult to discern between 5 and 10 atm, and for ϕ = 1.25-1.4, the model predicts very similar amounts of CO for all pressures.

5.3.2 Effect of Residence Time (p = 1 atm)

5.3.2.1 Flame Temperature

A plot of the adiabatic flame temperature for the oxidation of ethanol at varying mixture strengths is given in Figure 5.17 for residence times of 1, 5, and 10 ms. Temperatures peak at φ = 1.1 for τ = 5 and 10 ms, and at slightly richer conditions (ϕ = 1.15) for 1 ms. Approximate maximum values attained are 1989, 2078, and 2116 K for 1, 5, and 10 ms, respectively. Changes in temperatures corresponding to different residence times are relatively uniform throughout the entire ϕ range, although differences are slightly larger at stoichiometric than at extremely lean or rich mixtures. Increasing the charge duration in the reactor from 1 to 5 ms has a more substantial effect on flame temperature than does a change from 5 to 10 ms.

5.3.2.2 CO

The formation of CO over a range of ϕ = 0.6-1.4 is given in Figure 5.18 for τ = 1, 5, and 10 ms. CO levels again increase with equivalence ratio and vary only slightly with residence

time at rich conditions. The most substantial changes due to τ are at lean and stoichiometric mixtures. At ϕ = 1.0, y_{CO} = 0.032, 0.026, and 0.023, and at the lean end of the spectrum, 0.01, 0.004, and 0.003 for τ = 1, 5, and 10 ms, respectively.

5.4 Comparison of Fuels (p = 1 atm, τ = 5 ms)

Thus far, the effects of changing reactor pressure and charge residence time have been studied while isolating the fuel. In order to predict whether use of alternative fuels will be beneficial, combustion performance comparisons of flame temperature and exhaust gas species composition should be carried out. To this end, fuels are compared next in terms of their flame temperatures and emissions including CO, NO, CO_2, and H_2O. The latter two species have been included because of their contribution to greenhouse gases. The results presented are for atmospheric pressure with a residence time of 5 ms.

5.4.1 Flame Temperature

The adiabatic flame temperatures are compared in Figure 5.19 for the combustion of methane, isooctane, and ethanol with air for equivalence ratios of 0.6-1.4. Note that the highest temperatures are achieved with isooctane for all mixture strengths. Its peak temperature of approximately 2152 K at ϕ = 1.1 is about 70 K higher than those for methane and ethanol. Maximum temperatures observed for methane (2082 K) and ethanol (2078 K) exist at ϕ = 1.05 and 1.1, respectively. For lean conditions from ϕ = 0.6-0.7, methane and ethanol produce very similar values and those for isooctane are only about 35-50 K higher. From ϕ = 0.7-1.1, temperatures are slightly larger for methane than ethanol, while rich conditions beyond this range yield the opposite.

5.4.2 CO

CO formation is depicted in Figure 5.20 for the three fuels from ϕ = 0.6-1.4. It is observed that the highest levels of CO are generated through the combustion of isooctane for rich mixtures. This is intuitive considering the arguments previously made regarding the insufficient oxidation of carbon to eliminate CO. It should be expected that as the ratio of the number of hydrogen atoms in the fuel to the number of carbon atoms, H/C, decreases, CO levels would increase. Isooctane (C_8H_{18}) has the smallest H/C ratio and therefore the presence of more carbon atoms in the gas mixture return higher levels of y_{CO}. Ethanol (C_2H_5OH) follows isooctane in H/C ratio, and the results of CO formation are consistent with expectations despite the existence of oxygen in the molecule. Methane produces the smallest amount of CO for the entire range of ϕ. For stoichiometric and lean mixtures, ethanol generates higher y_{CO} than isooctane though quantities are similar for all three fuels.

Perhaps a more useful comparison of fuel emissions is given when the pollutant species are normalized with respect to energy available in the reactant fuel. Figure 5.21 depicts mass of CO produced normalized by the fuel energy input, or specific CO in grams/Joules, for ϕ = 0.6-1.4. Table 5.1 gives the corresponding fuel energy, in Joules, entering the reactor for each equivalence ratio. Isooctane is observed to have the highest levels of specific CO for $\phi \geq 1.1$, while for $\phi \leq 1.05$, ethanol yields the largest quantities. The oxidation of methane generates the smallest specific CO emissions for all ϕ. Numerical values corresponding to Figure 5.21 are given in Table A.1 in Appendix A. For example, values at ϕ = 1.0 are 7.31, 8.85, and 9.54 g/MJ for methane, isooctane, and ethanol, respectively. Qualitatively, these results are very similar to those for y_{CO} shown in Figure 5.20.

Note that the energy input associated with each fuel presented in Table 5.1 is very nearly the same for a given equivalence ratio. This is a result of different quantities of fuel in the inlet mixture. Table 5.2 gives the number of moles of fuel entering the reactor at each ϕ. Because the reactor volume, pressure, and residence time have been constrained, smaller amounts of the large molecule fuels will enter the reactor than those smaller in size. Table 5.1 reveals that isooctane, which has the largest LHV on a molar basis, provides approximately the same energy input as methane, which has the smallest molar LHV. The specific emissions of each species, however, will be the same regardless of the amount of fuel entering the reactor.

Table 5.1: Fuel Energy Input into Reactor.

	Fuel Energy Input (J)		
ϕ	Methane	Isooctane	Ethanol
0.60	72.35	74.28	73.09
0.65	96.28	96.32	96.27
0.70	98.11	98.05	98.41
0.75	100.03	99.90	100.59
0.80	102.05	101.91	102.79
0.85	104.20	104.07	105.06
0.90	106.52	106.45	107.40
0.95	109.07	109.09	109.87
1.00	111.91	112.04	112.50
1.05	115.13	115.37	115.37
1.10	118.79	119.60	118.54
1.15	122.94	123.49	122.08
1.20	127.58	128.33	126.04
1.25	132.62	133.30	130.41
1.30	137.99	138.81	135.14
1.35	143.59	144.59	140.14
1.40	149.34	150.58	145.34

Table 5.2: Moles of Fuel Entering Reactor.

	Moles Entering Reactor		
ϕ	Methane	Isooctane	Ethanol
0.60	9.02×10^{-5}	1.47×10^{-5}	5.90×10^{-5}
0.65	1.20×10^{-4}	1.90×10^{-5}	7.77×10^{-5}
0.70	1.22×10^{-4}	1.94×10^{-5}	7.94×10^{-5}
0.75	1.25×10^{-4}	1.97×10^{-5}	8.12×10^{-5}
0.80	1.27×10^{-4}	2.01×10^{-5}	8.29×10^{-5}
0.85	1.30×10^{-4}	2.06×10^{-5}	8.48×10^{-5}
0.90	1.33×10^{-4}	2.10×10^{-5}	8.67×10^{-5}
0.95	1.36×10^{-4}	2.16×10^{-5}	8.87×10^{-5}
1.00	1.40×10^{-4}	2.21×10^{-5}	9.08×10^{-5}
1.05	1.44×10^{-4}	2.28×10^{-5}	9.31×10^{-5}
1.10	1.48×10^{-4}	2.36×10^{-5}	9.56×10^{-5}
1.15	1.53×10^{-4}	2.44×10^{-5}	9.85×10^{-5}
1.20	1.59×10^{-4}	2.54×10^{-5}	1.02×10^{-4}
1.25	1.65×10^{-4}	2.63×10^{-5}	1.05×10^{-4}
1.30	1.72×10^{-4}	2.74×10^{-5}	1.09×10^{-4}
1.35	1.79×10^{-4}	2.86×10^{-5}	1.13×10^{-4}
1.40	1.86×10^{-4}	2.98×10^{-5}	1.17×10^{-4}

5.4.3 NO

The formation of NO is shown in Figure 5.22 for methane and isooctane from ϕ = 0.6-1.4. Significantly higher levels of NO are generated from isooctane combustion for all mixtures except those that are extremely lean where variations are small. A difference of over 270 ppm is observed between peak values, which for both fuels occurs at ϕ = 1.05 near peak temperatures (recall Figure 5.19). The shapes of the curves also reinforce the notion that temperature is the primary factor governing NO formation. Figure 5.19 shows that temperature differences between methane and isooctane are actually quite uniform throughout the ϕ range. The nonlinear relationship between temperature and initial NO formation given in Eq. (5.5) from the extended Zeldovich mechanism explains why the differences in NO are not uniform, but largest at the highest temperatures. The differences in NO formation between fuels at extremely lean

and rich conditions are also observed to scale according to their absolute temperature magnitudes.

Specific NO emissions for methane and isooctane are shown in Figure 5.23 for ϕ = 0.6-1.4 and tabulated in Table A.2. Similar to y_{NO} of Figure 5.22, specific NO levels are significantly larger for isooctane than for methane for the entire range of ϕ except at extremely lean mixtures where quantities are small. Peak levels are approximately 0.066 and 0.169 g/MJ for methane and isooctane, respectively.

5.4.4 CO_2

The production of CO_2 for the three fuels is represented in Figure 5.24 over ϕ = 0.6-1.4. The most significant quantities of CO_2 are observed from ϕ = 0.9-1.0 for each fuel. Maximum values of y_{CO_2} are approximately 0.074, 0.094, and 0.098 for methane, ethanol, and isooctane, respectively. Isooctane generates the highest levels followed by ethanol and methane for $\phi \leq$ 1.1. However, beyond this point ethanol surpasses isooctane in CO_2 production. The likely cause of this is the presence of an additional oxygen atom in the molecular structure of ethanol. The smallest CO_2 mole fractions are at ϕ = 1.4, which supports the argument for maximum CO production at rich conditions.

Figure 5.25 gives the specific CO_2 emissions for the three fuels from ϕ = 0.6-1.4. Isooctane and ethanol generate about the same amount of specific CO_2 for $\phi \leq 1.05$; beyond this point higher levels are seen for ethanol combustion. Methane produces the least specific CO_2 for all mixtures. Numerical values are tabulated in Table A.3. At ϕ = 1.0 values are about 42.4 g/MJ for methane and 54.6 g/MJ for isooctane and ethanol. Note that as opposed to specific CO and NO formation given in Figures 5.21 and 5.23, significant quantities of CO_2 are generated for all mixture strengths. CO_2, H_2O, and N_2 constitute the only products of complete combustion of

a hydrocarbon fuel with air; considerable amounts will therefore always be produced regardless of whether or not combustion is complete.

5.4.5 H_2O

Figure 5.26 gives the H_2O production for each fuel over ϕ = 0.6-1.4. The largest y_{H_2O} values occur at rich conditions beyond ϕ = 1.1. Maximums are approximately 0.135, 0.179, and 0.181 for isooctane, ethanol, and methane, respectively. Methane generates the highest y_{H_2O} for the majority of mixture strengths ($0.6 \leq \phi \leq 1.25$), though values for ethanol are similar and actually surpass those of methane beyond ϕ = 1.25. This again illustrates the impact of fuel H/C ratio on emissions. Isooctane has the smallest H/C ratio and generates the lowest H_2O levels as would be expected from analogous arguments on CO formation made in section 5.4.2. Also note that the presence of oxygen in the chemical structure of ethanol will generally contribute to larger levels of species composed of oxygen in rich conditions than non-oxygenated fuels. H_2O, like CO_2, will always be a product of hydrocarbon combustion and therefore appears in significant quantities for all mixture strengths.

Specific H_2O emissions for each fuel are presented in Figure 5.27 over ϕ = 0.6-1.4 and tabulated in Table A.4. Methane generates the largest specific H_2O levels for the majority of mixtures except very rich where it is surpassed by ethanol. Production from isooctane oxidation is the least for all ϕ. Values at ϕ = 1.0 are approximately 29.1, 39.3, and 40.8 g/MJ for isooctane, ethanol, and methane, respectively.

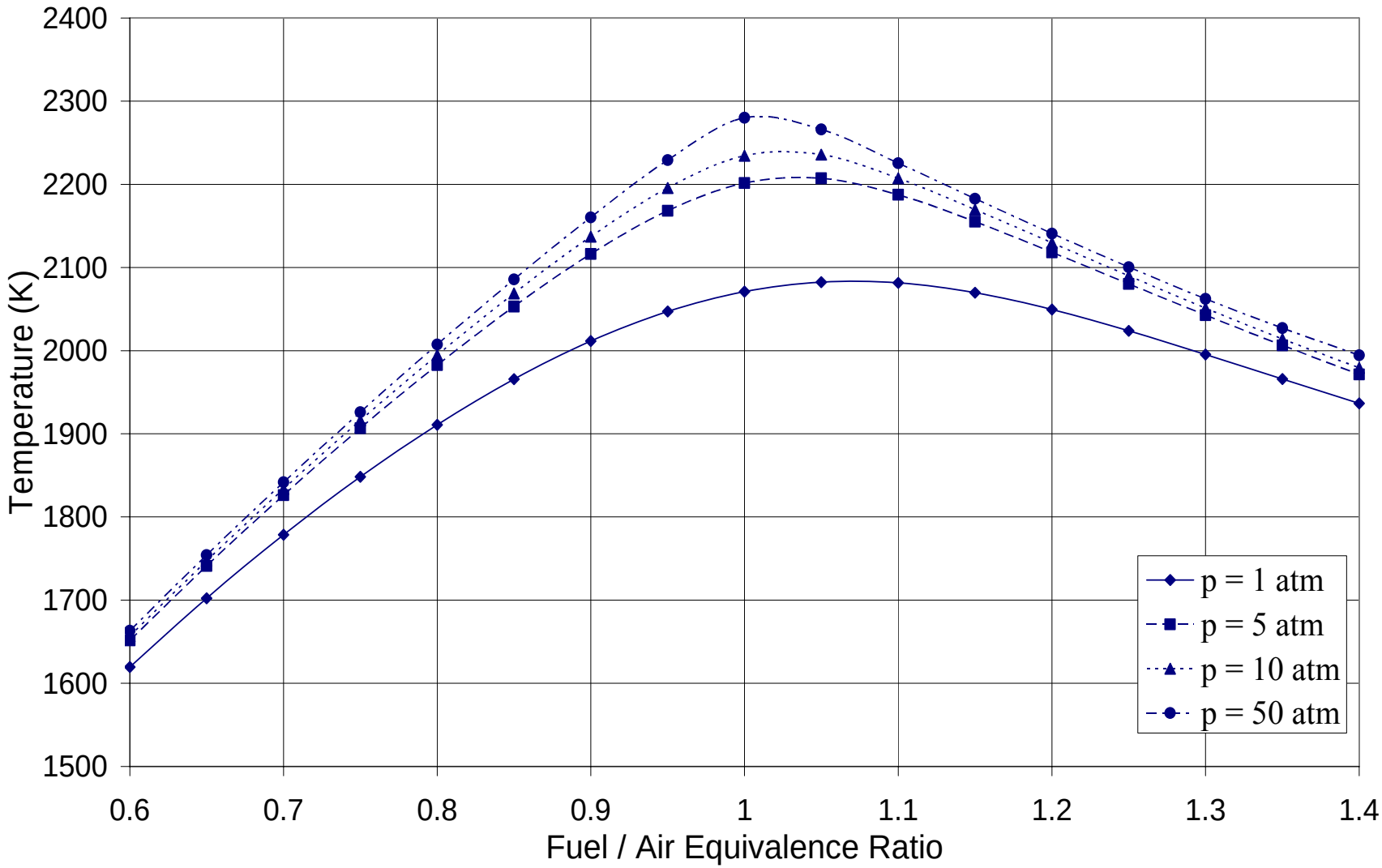

Figure 5.1: Effect of Pressure on Adiabatic Flame Temperature for Methane-Air PSR, τ = 5 ms

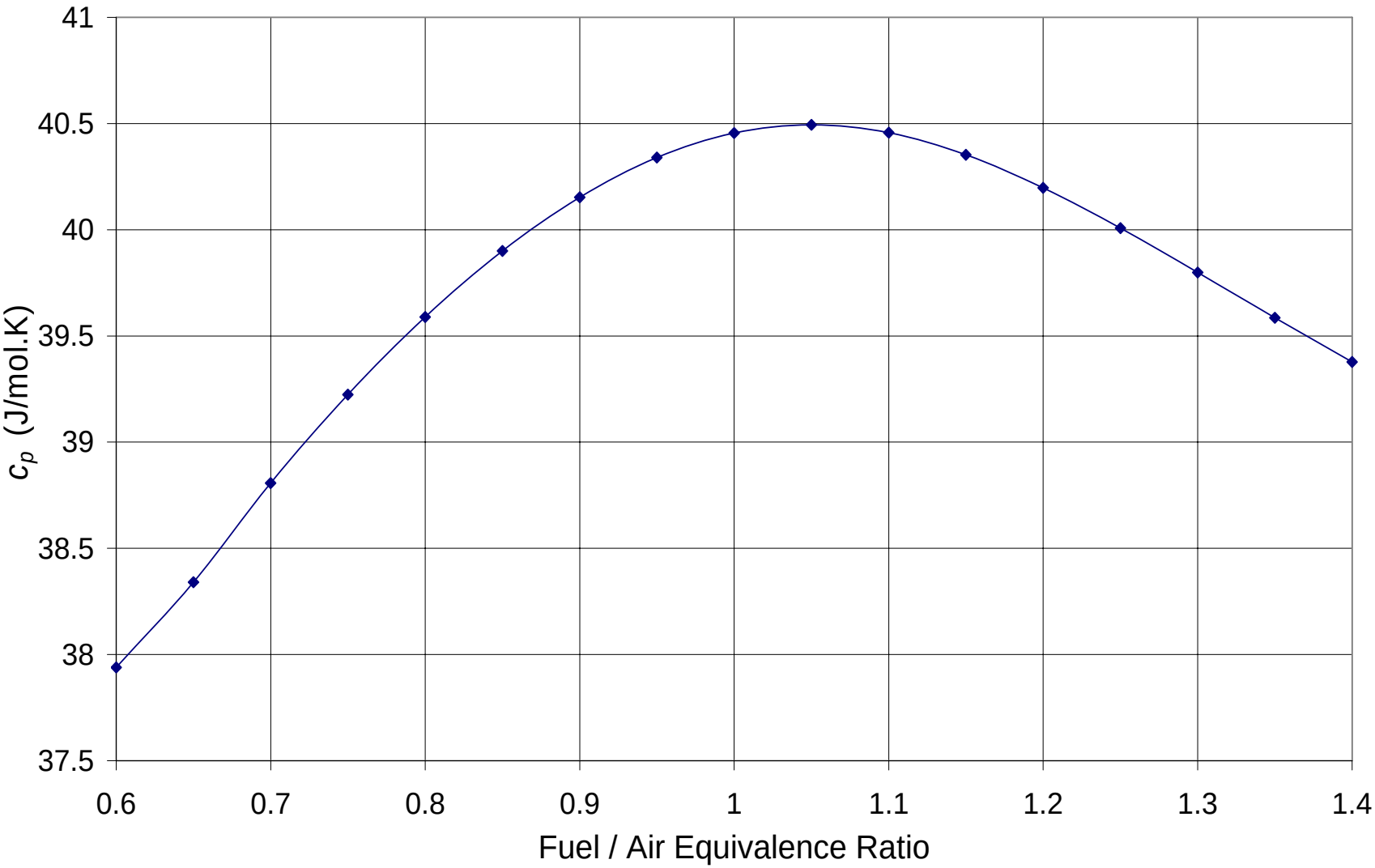

Figure 5.2: Specific Heat of Product Mixture for Methane-Air PSR, p = 1 atm, τ = 5 ms

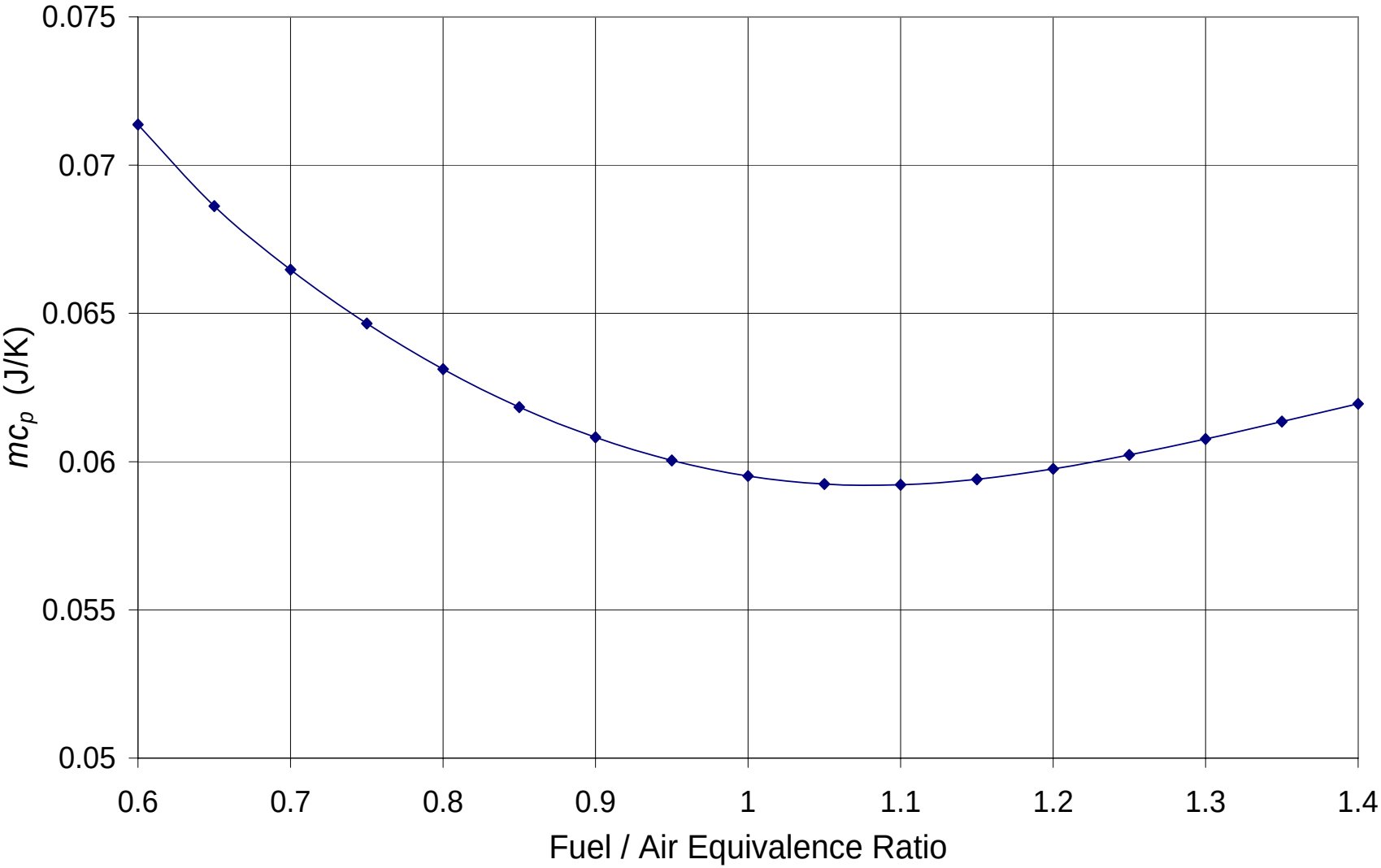

Figure 5.3: mc_p of Product Mixture for Methane-Air PSR, p = 1 atm, τ = 5 ms

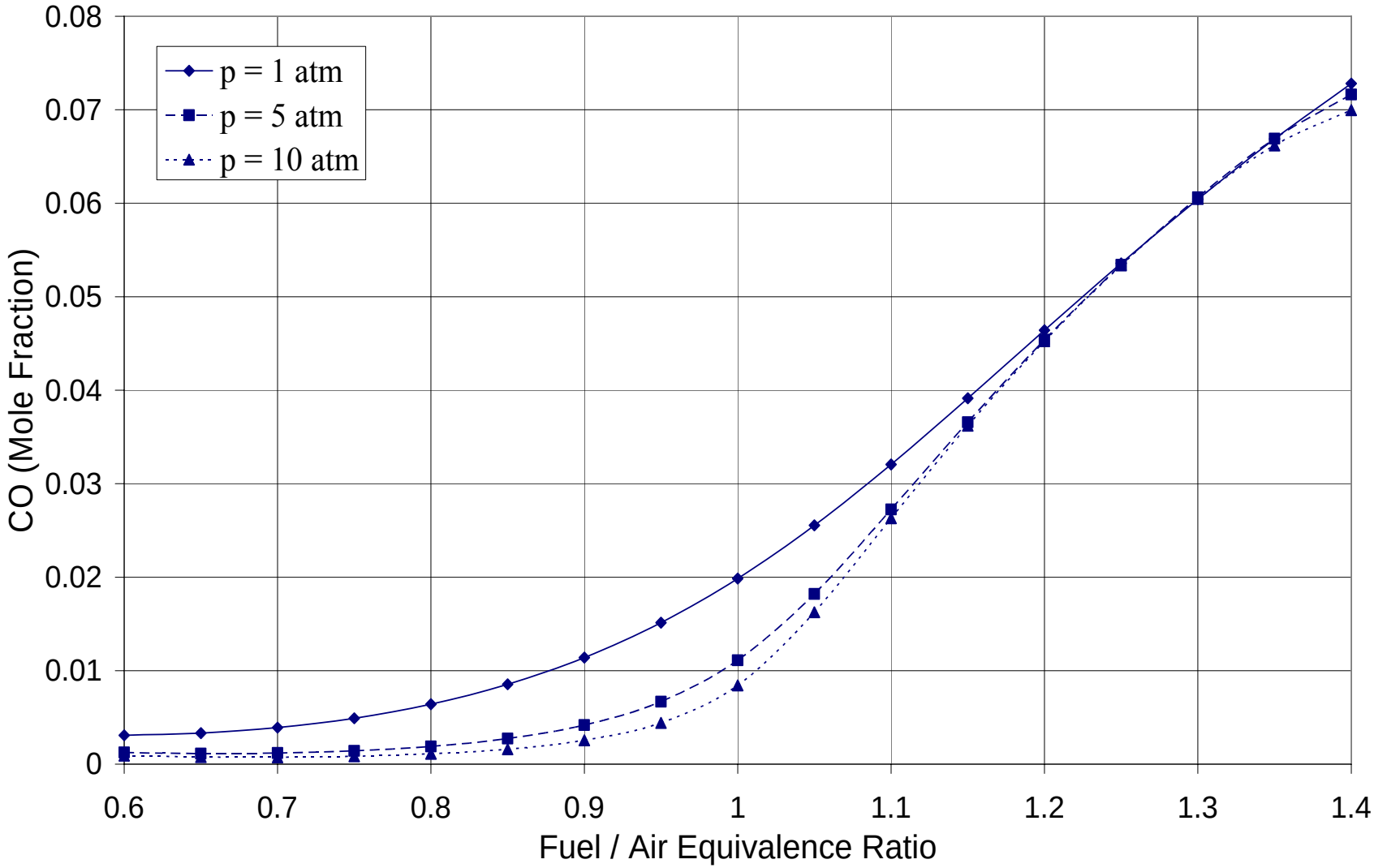

Figure 5.4: Effect of Pressure on CO Formation for Methane-Air PSR, $\tau = 5$ ms

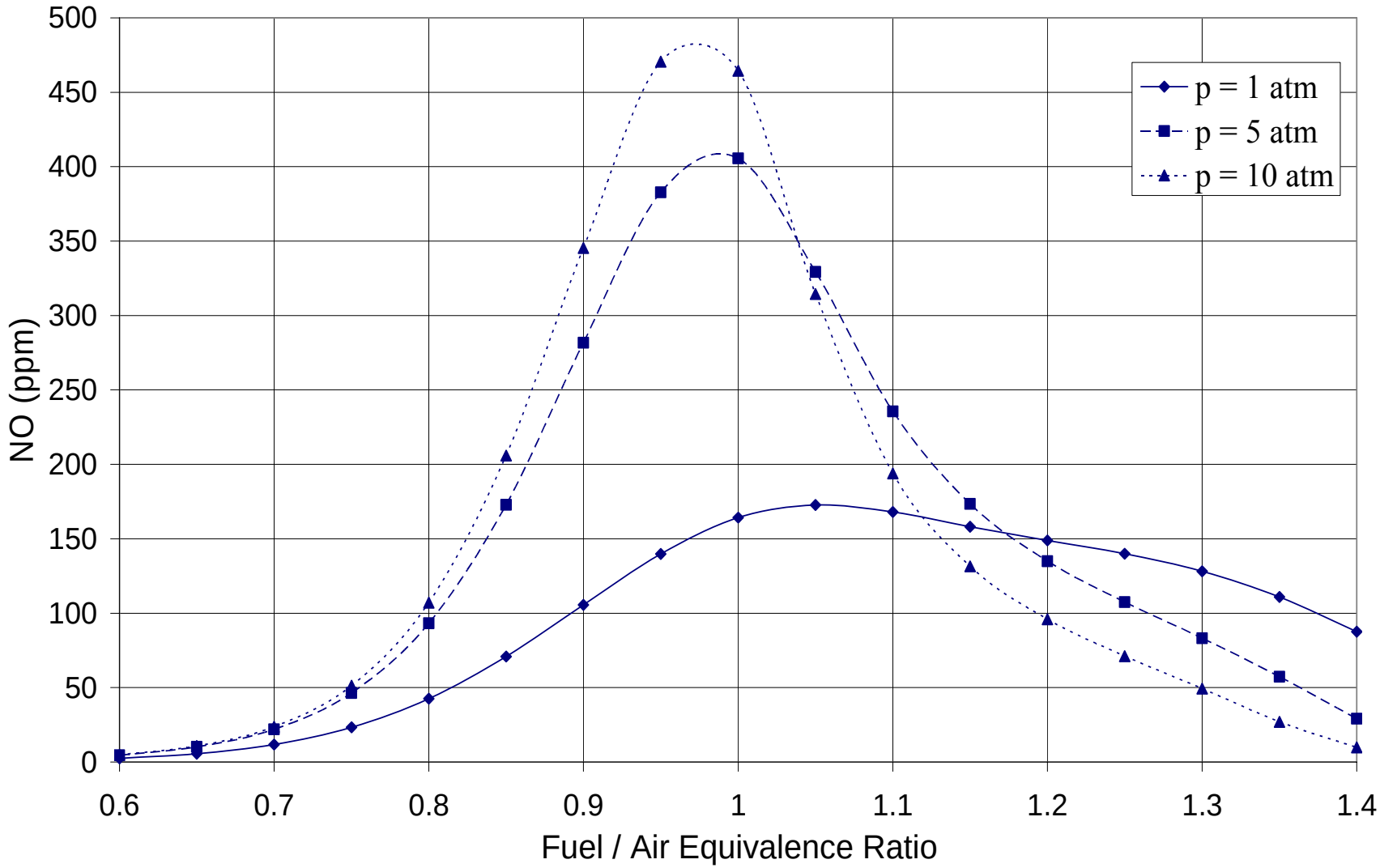

Figure 5.5: Effect of Pressure on NO Formation for Methane-Air PSR, τ = 5 ms

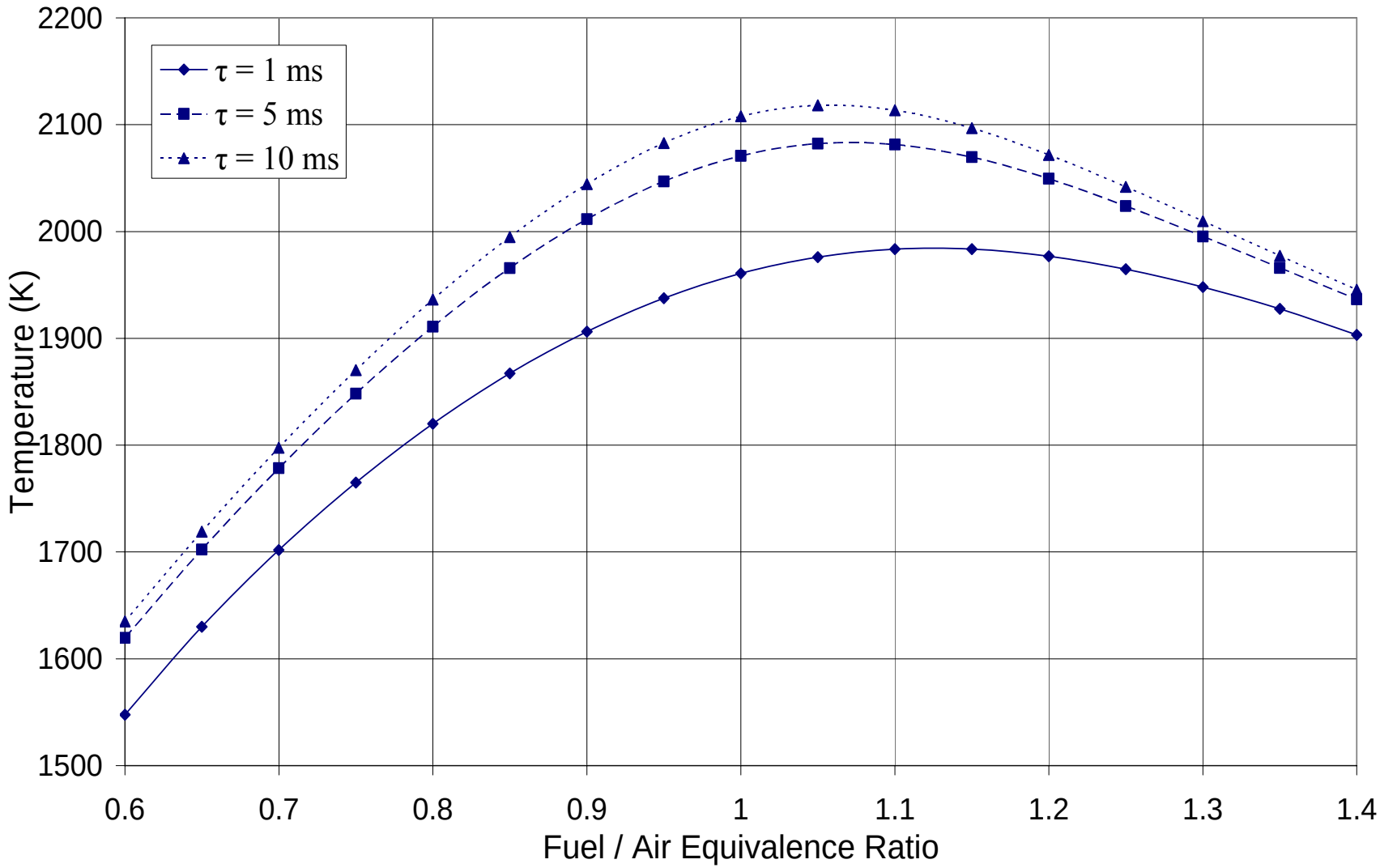

Figure 5.6: Effect of Residence Time on Adiabatic Flame Temperature for Methane-Air PSR, p = 1 atm

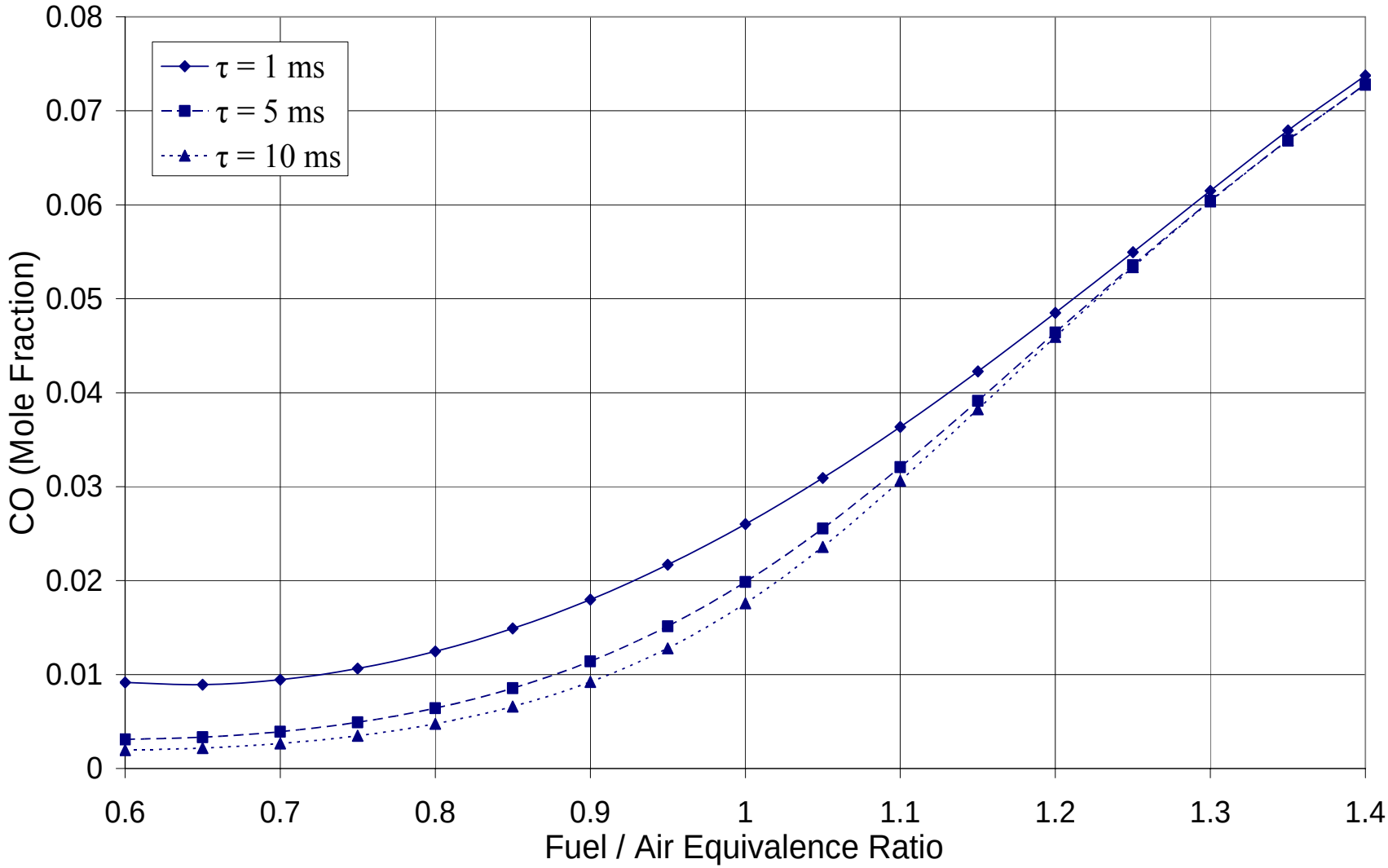

Figure 5.7: Effect of Residence Time on CO Formation for Methane-Air PSR, p = 1 atm

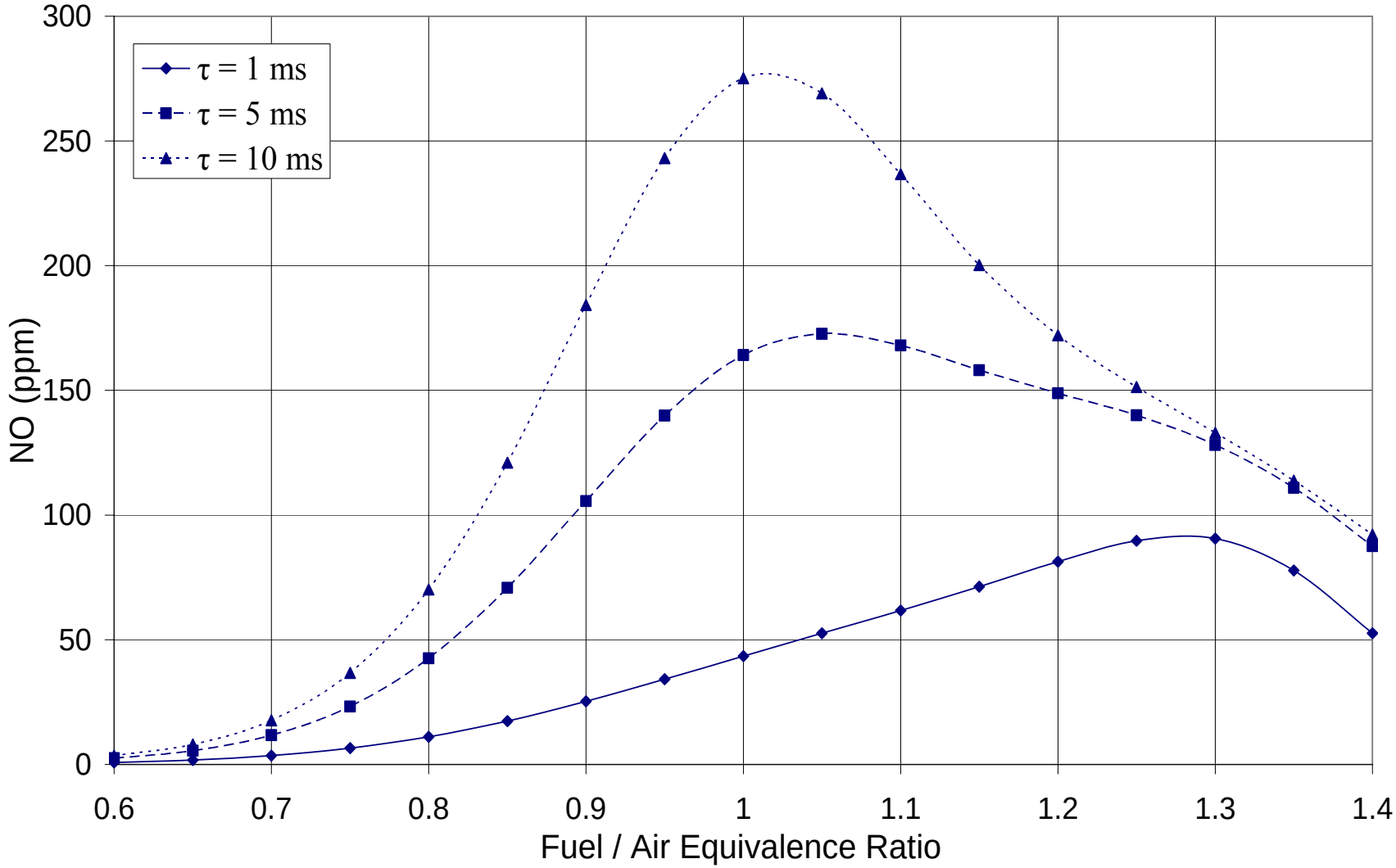

Figure 5.8: Effect of Residence Time on NO Formation for Methane-Air PSR, p = 1 atm

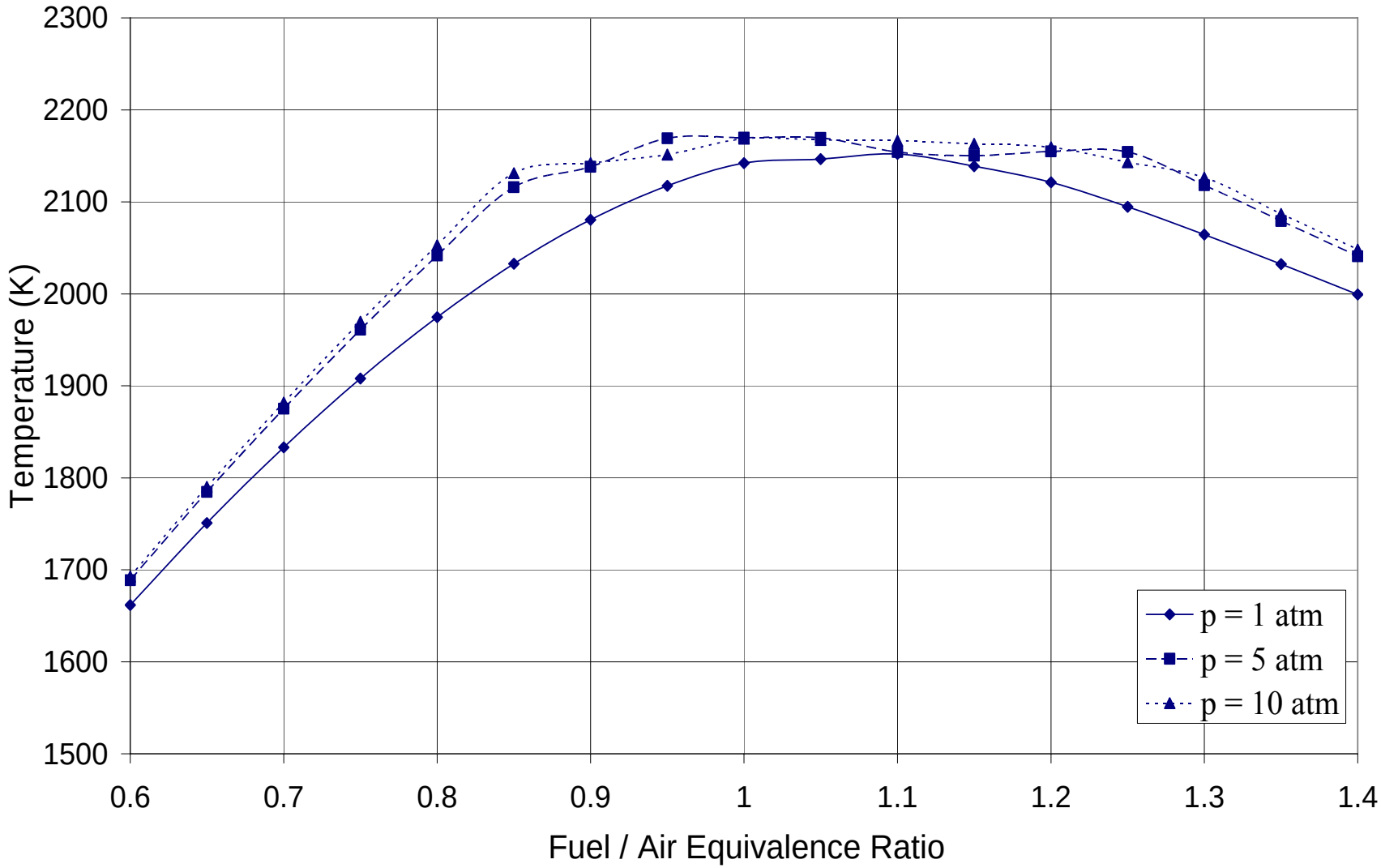

Figure 5.9: Effect of Pressure on Adiabatic Flame Temperature for Isooctane-Air PSR, τ = 5 ms

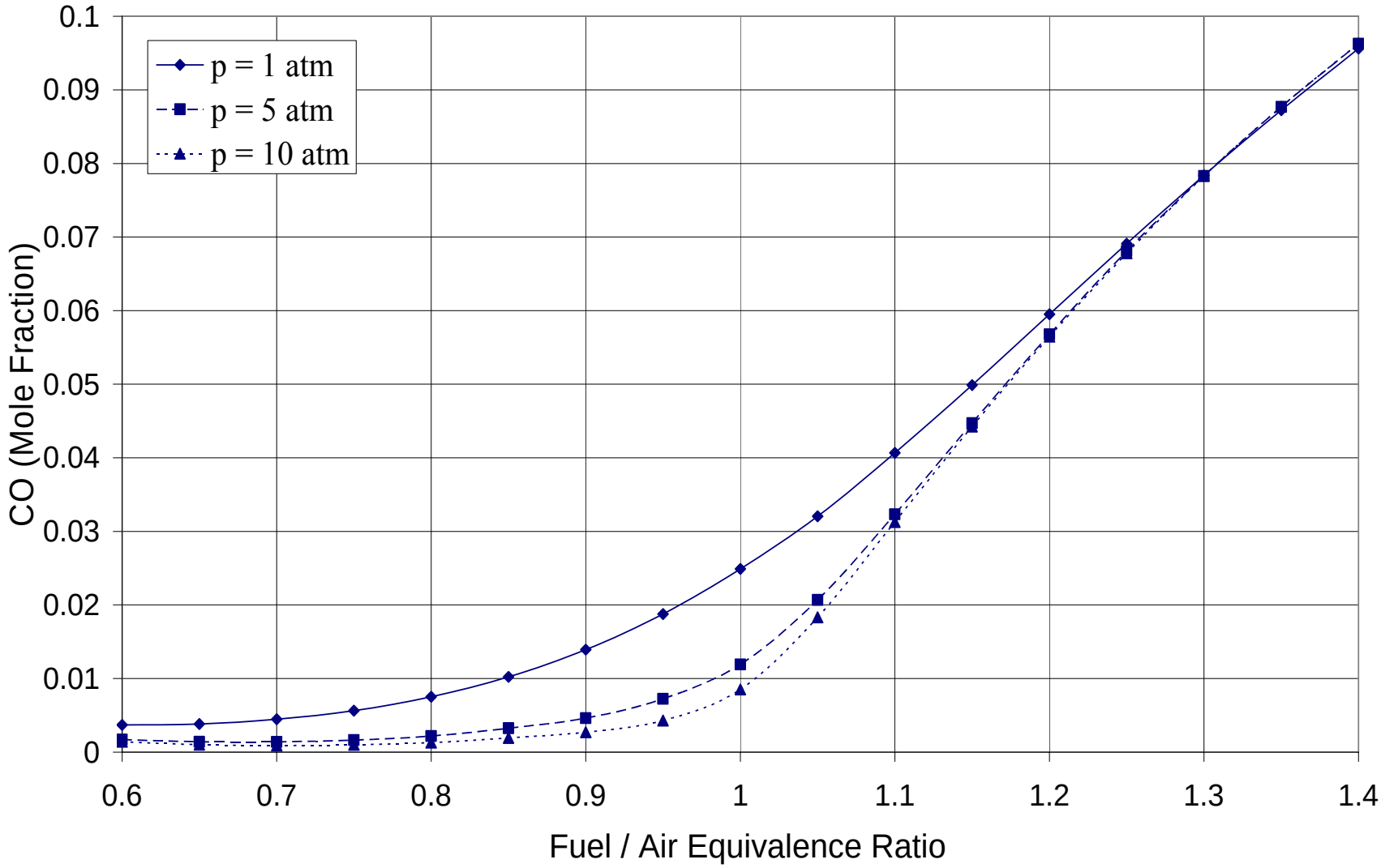

Figure 5.10: Effect of Pressure on CO Formation for Isooctane-Air PSR, τ = 5 ms

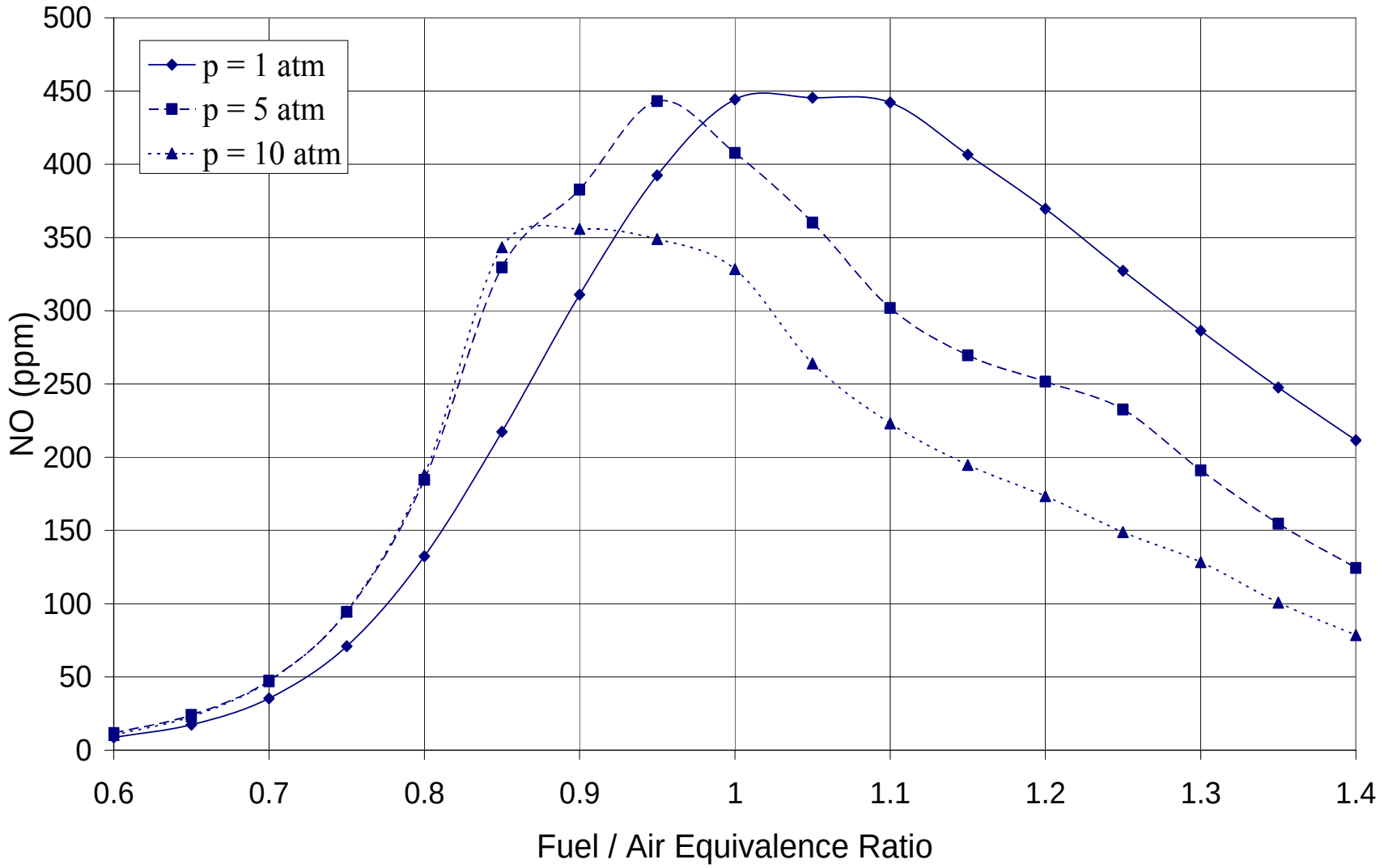

Figure 5.11: Effect of Pressure on NO Formation for Isooctane-Air PSR, τ = 5 ms

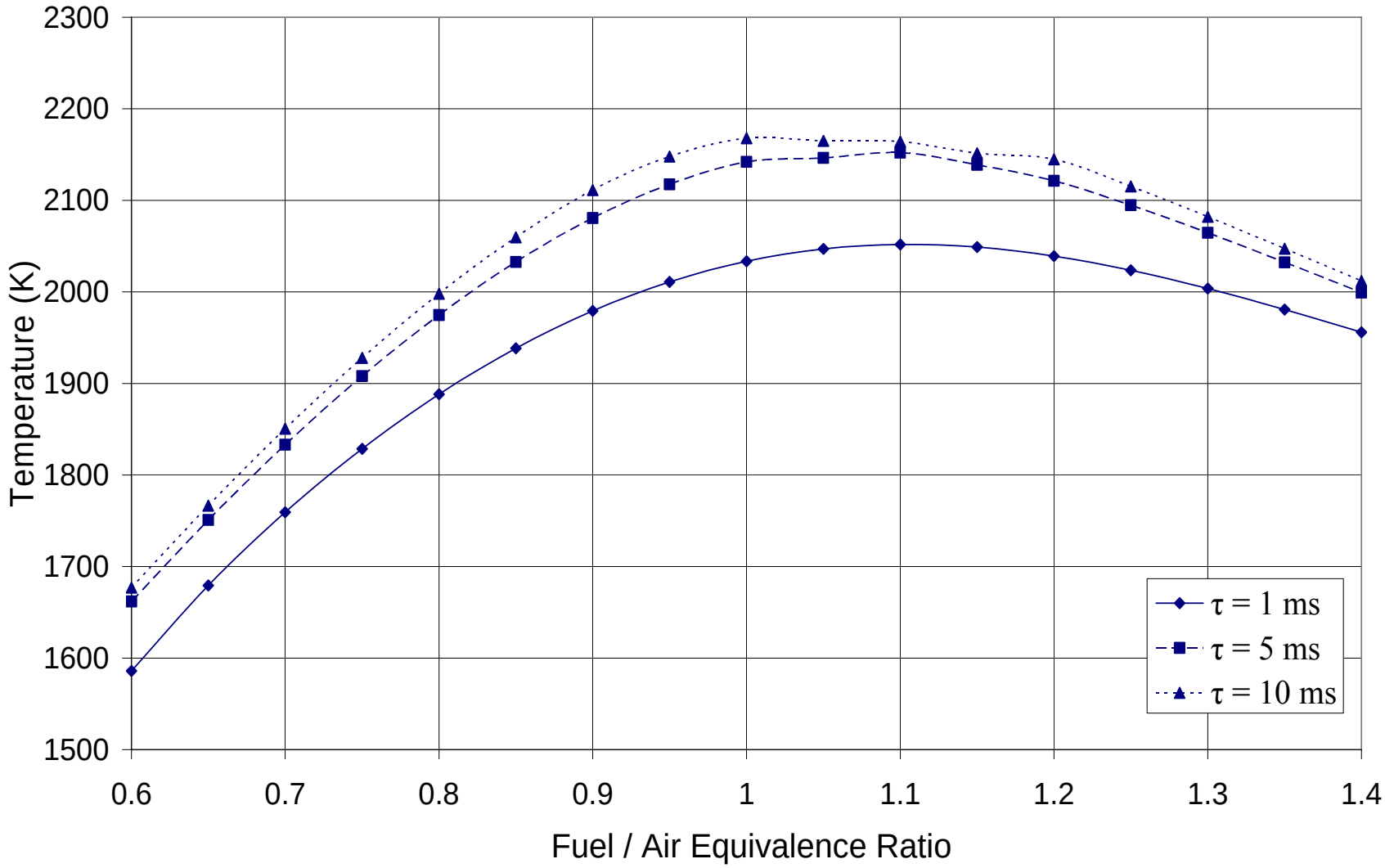

Figure 5.12: Effect of Residence Time on Adiabatic Flame Temperature for Isooctane-Air PSR, p = 1 atm

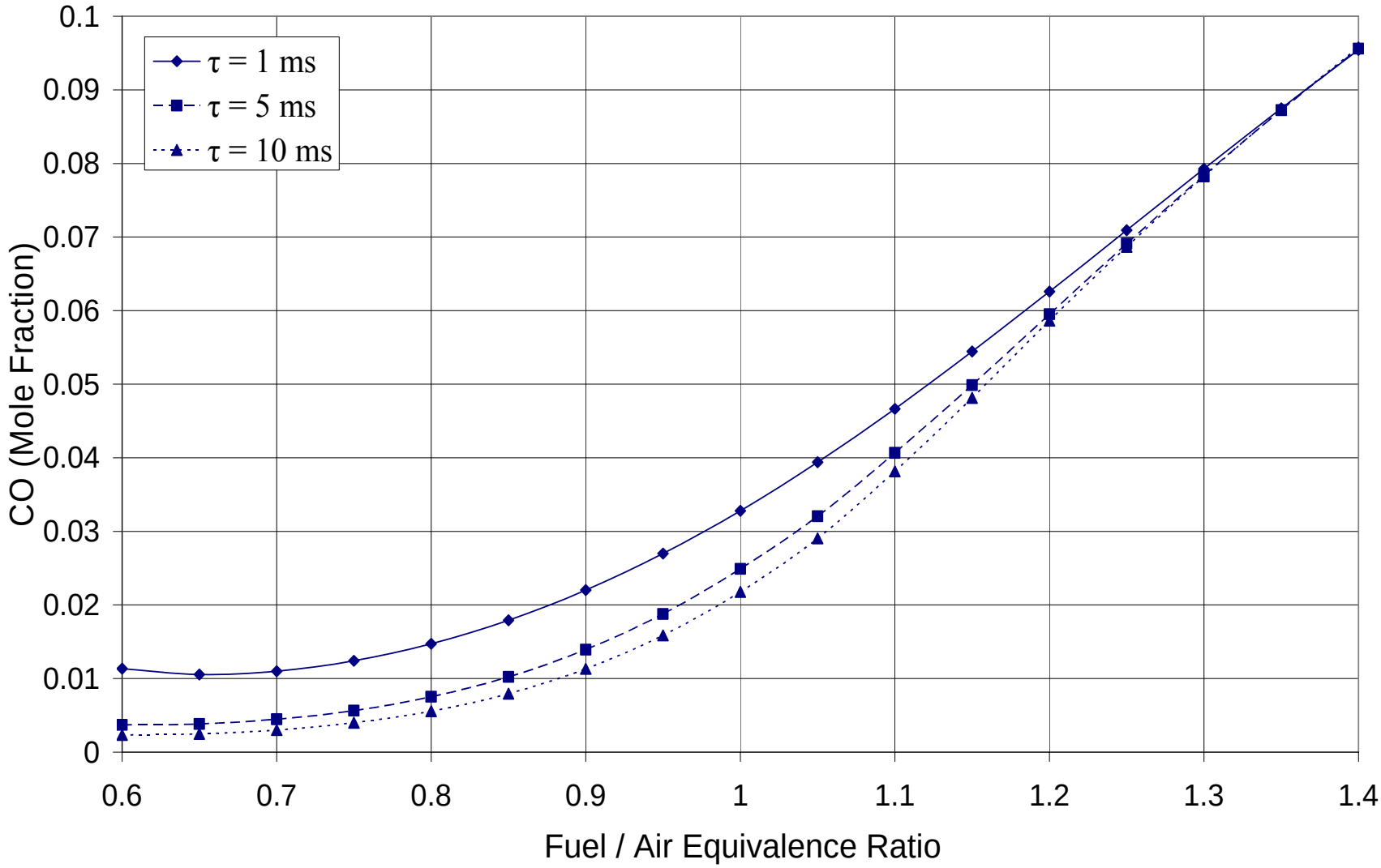

Figure 5.13: Effect of Residence Time on CO Formation for Isooctane-Air PSR, p = 1 atm

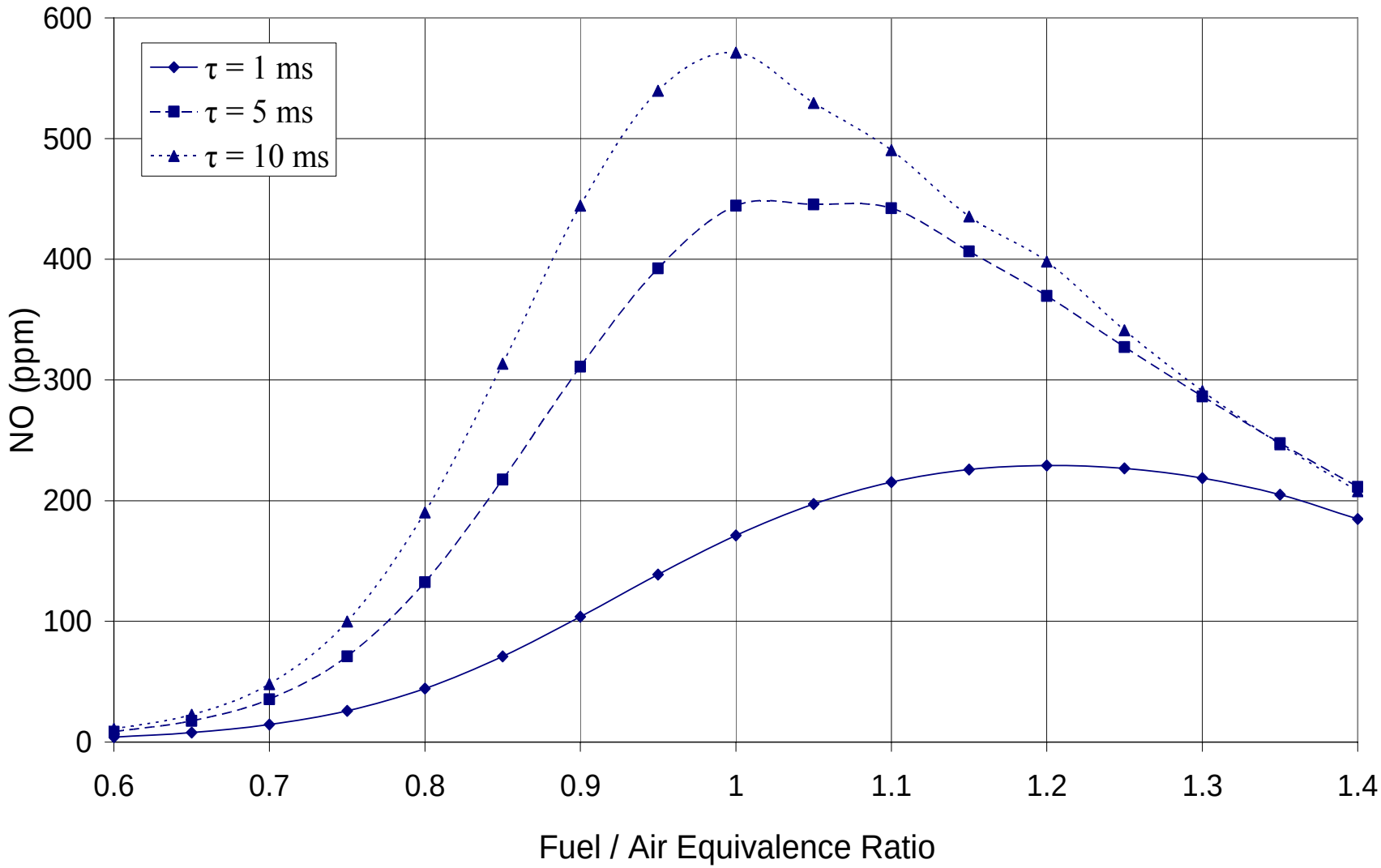

Figure 5.14: Effect of Residence Time on NO Formation for Isooctane-Air PSR, p = 1atm

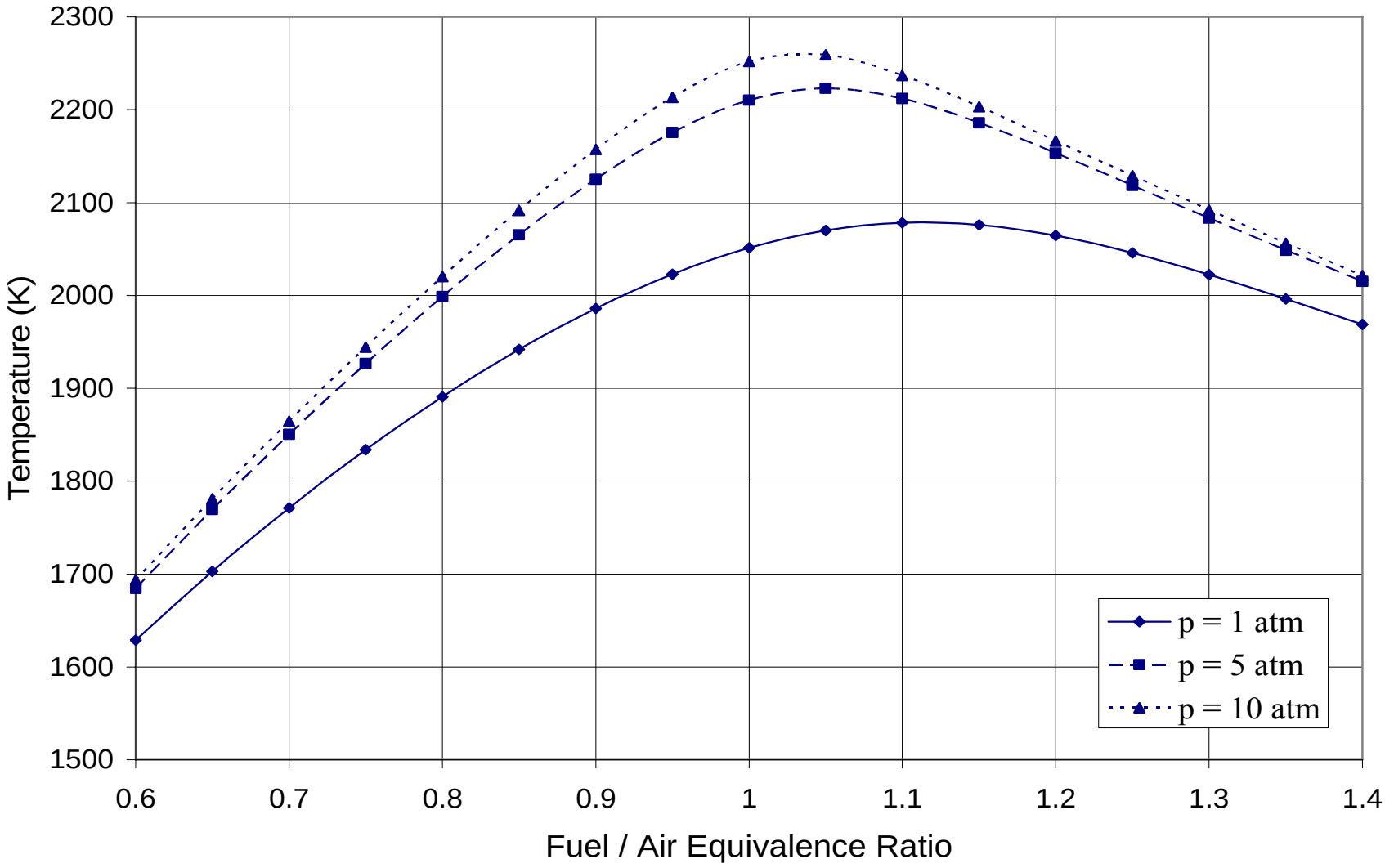

Figure 5.15: Effect of Pressure on Adiabatic Flame Temperature for Ethanol-Air PSR, $\tau = 5$ ms

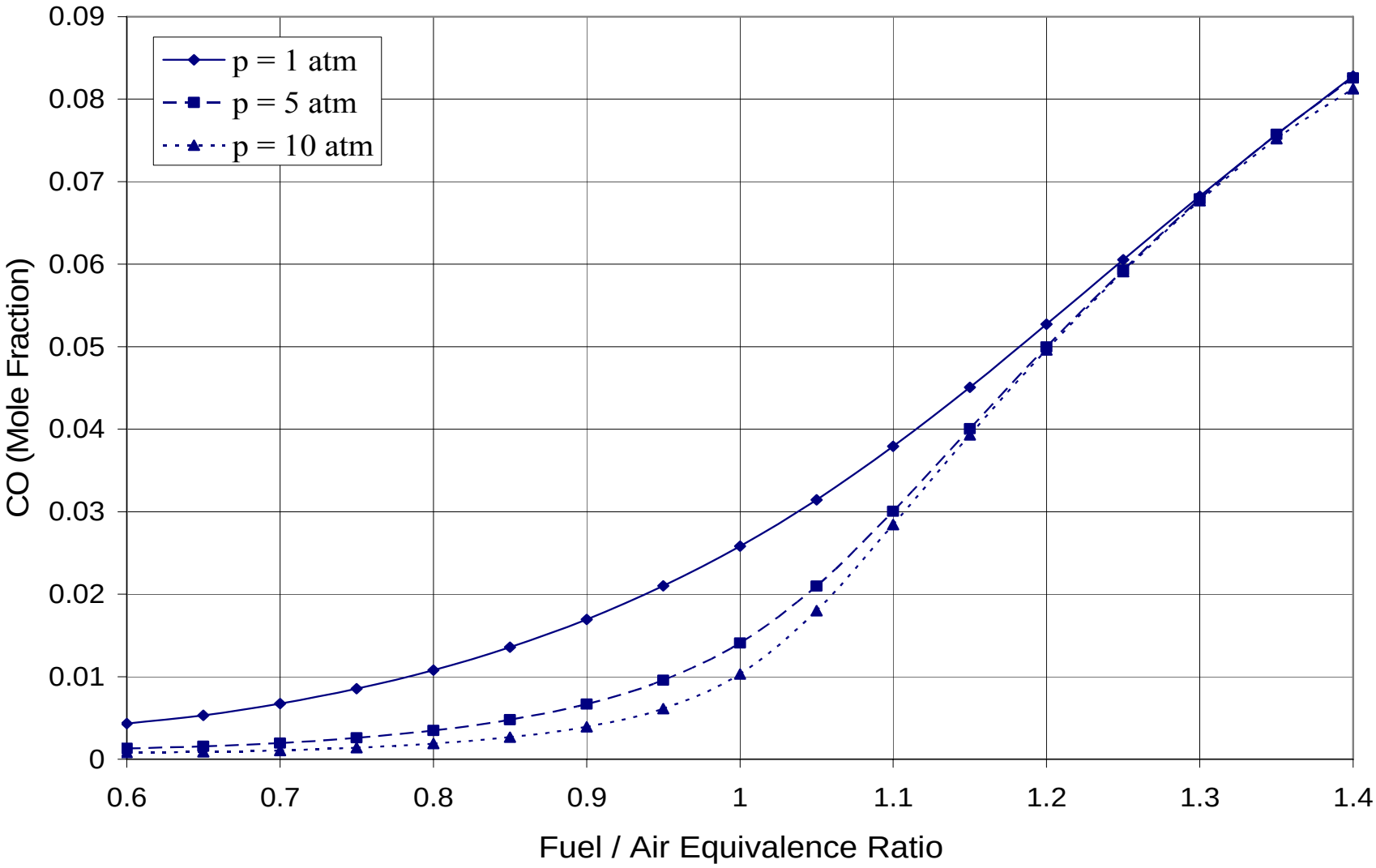

Figure 5.16: Effect of Pressure on CO Formation for Ethanol-Air PSR, τ = 5 ms

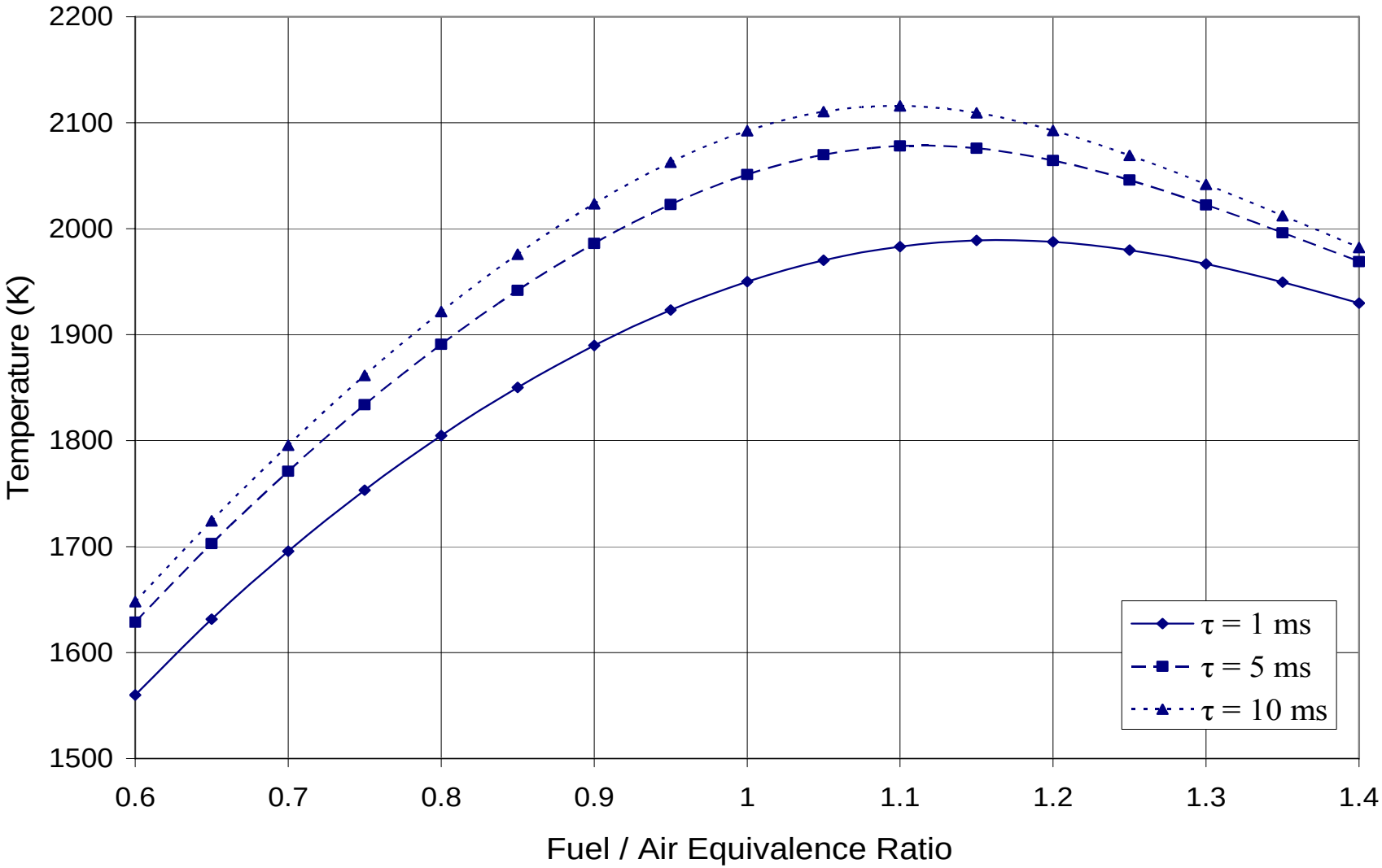

Figure 5.17: Effect of Residence Time on Adiabatic Flame Temperature for Ethanol-Air PSR, p = 1 atm

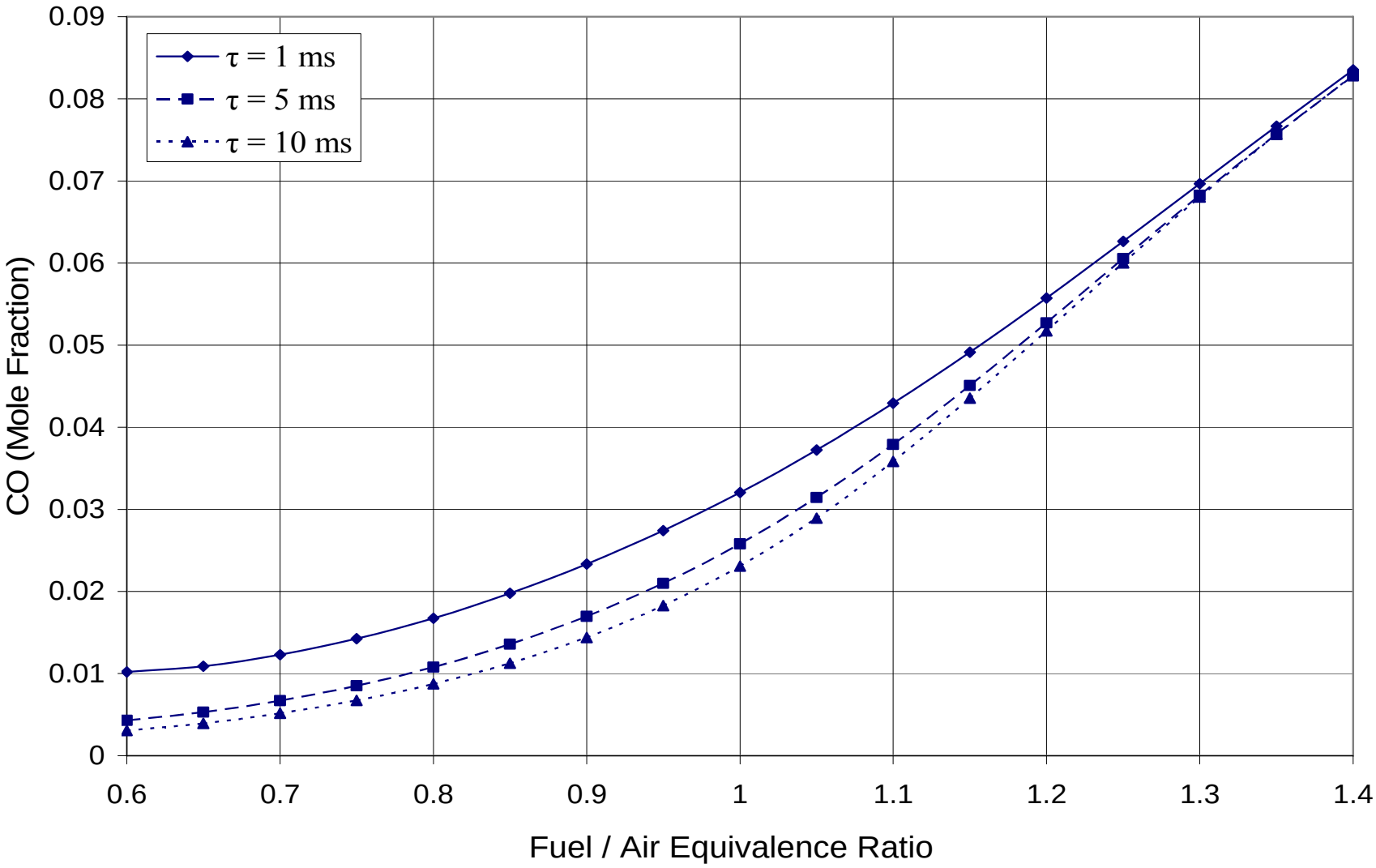

Figure 5.18: Effect of Residence Time on CO Formation for Ethanol-Air PSR, p = 1 atm

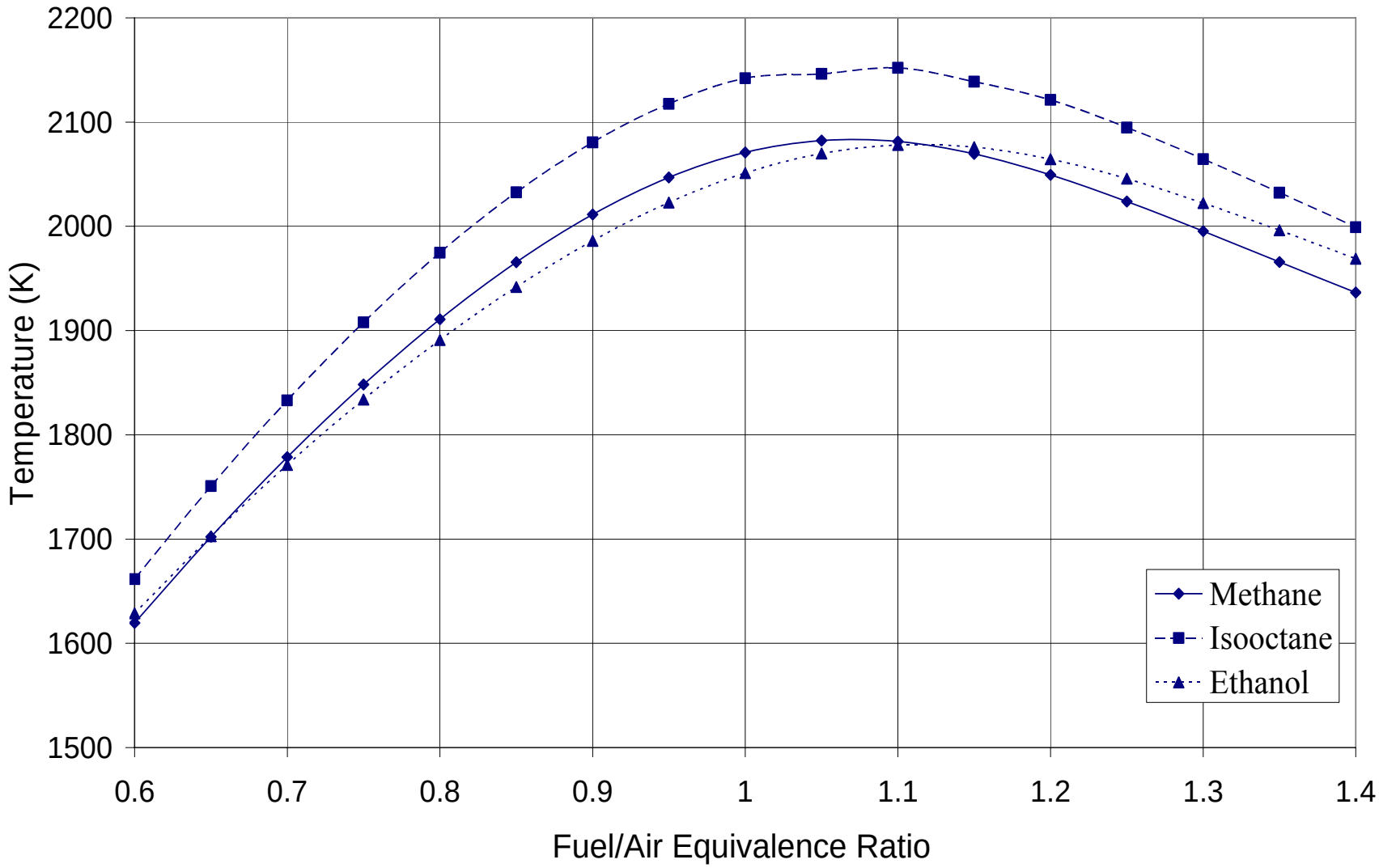

Figure 5.19: Adiabatic Flame Temperature from the Combustion of Three Fuels in a PSR, p = 1 atm, τ = 5 ms

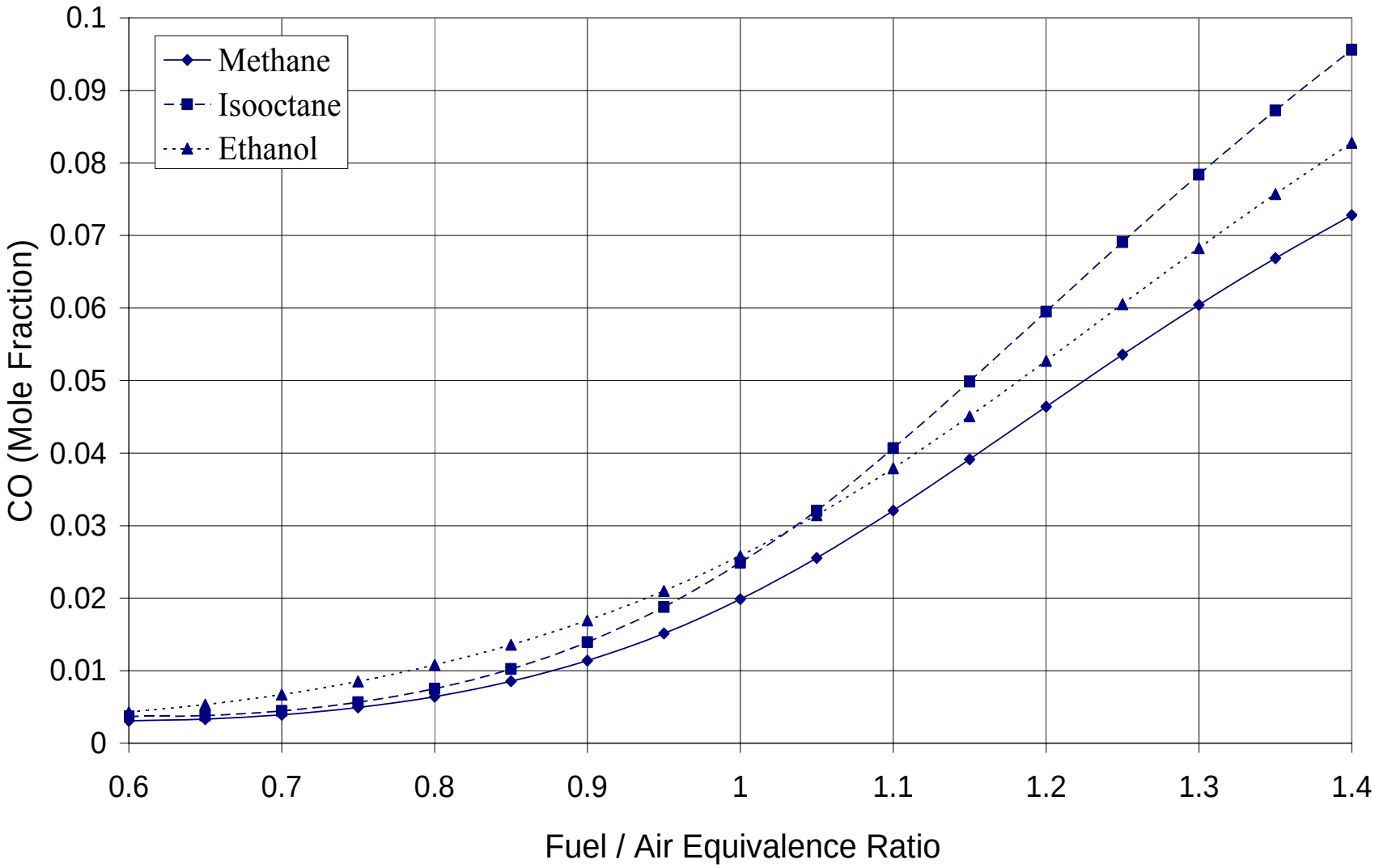

Figure 5.20: CO Formation from the Combustion of Three Fuels in a PSR, p = 1 atm, τ = 5 ms

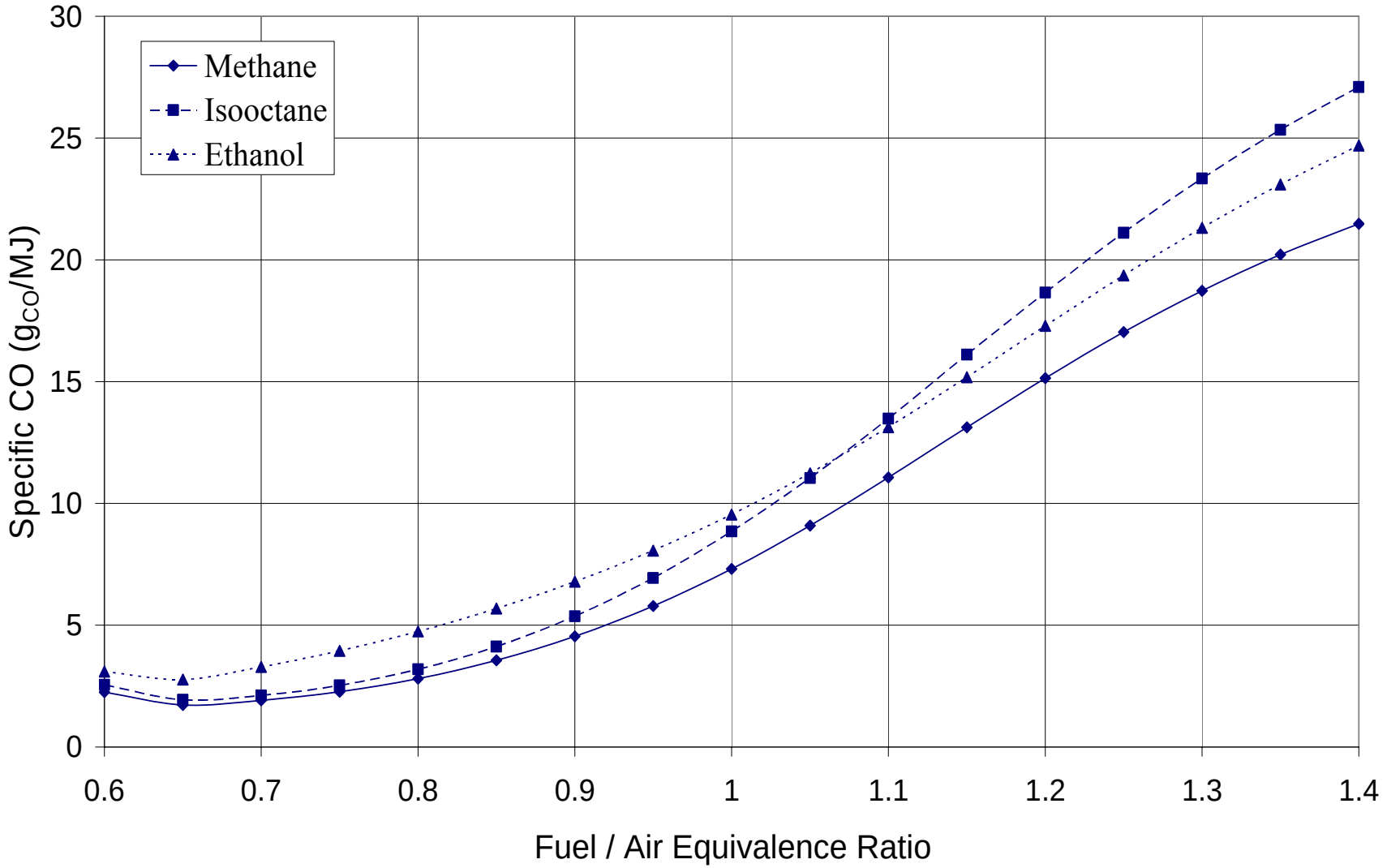

Figure 5.21: Specific Emissions of CO from the Combustion of Three Fuels in a PSR, p = 1 atm, τ = 5 ms

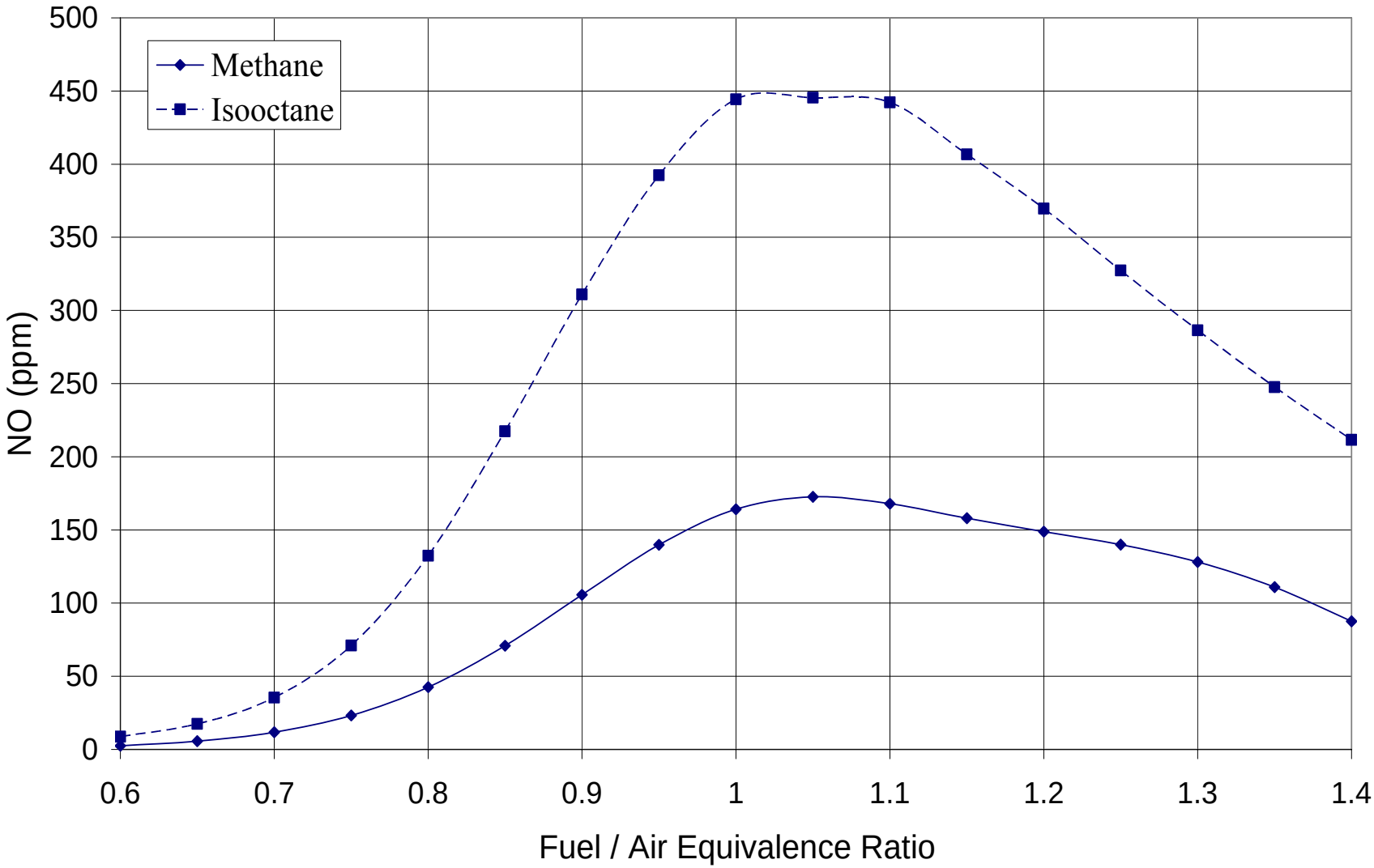

Figure 5.22: NO Formation from the Combustion of Two Fuels in a PSR, p = 1 atm, τ = 5 ms

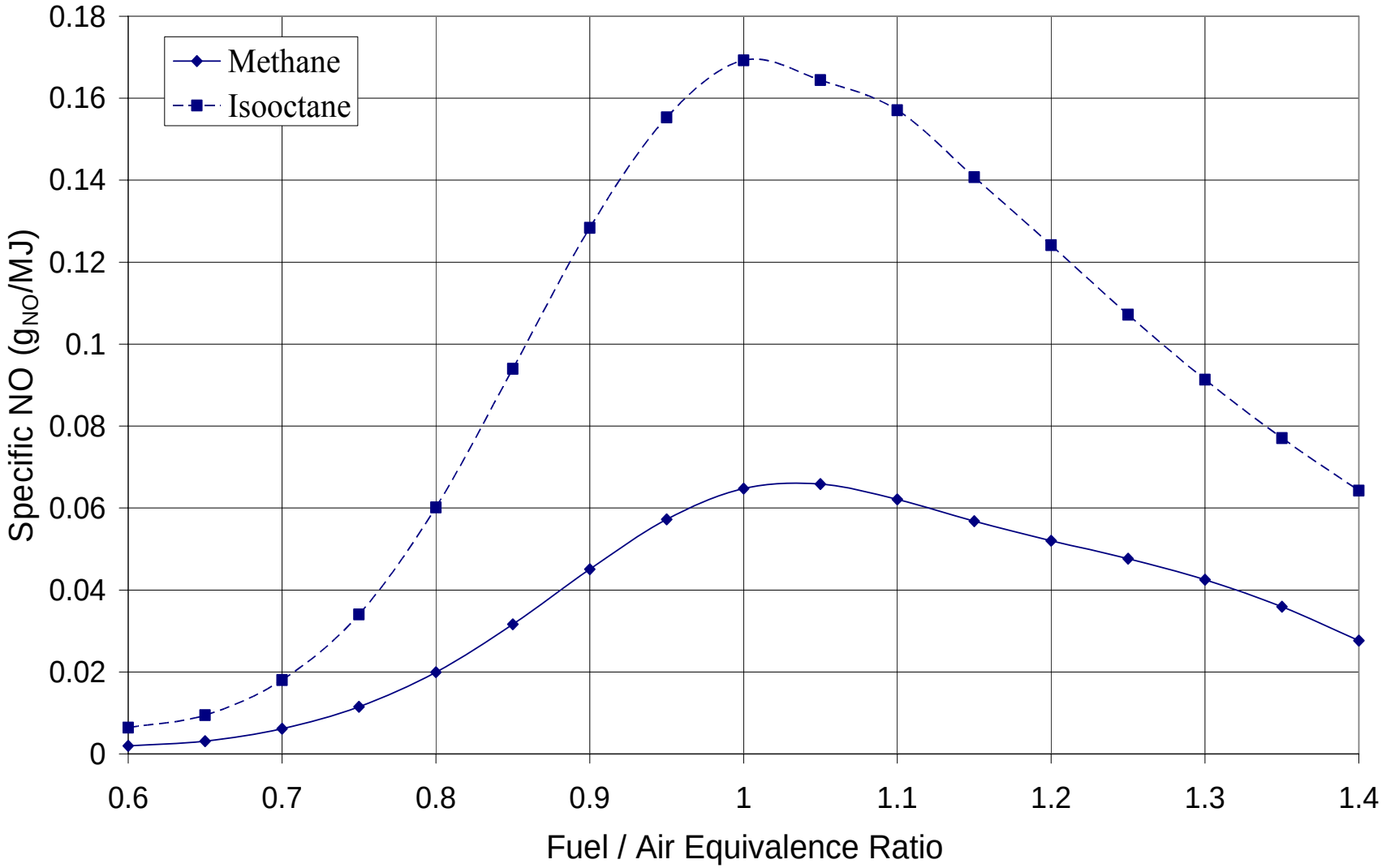

Figure 5.23: Specific Emissions of NO from the Combustion of Two Fuels in a PSR, p = 1 atm, τ = 5 ms

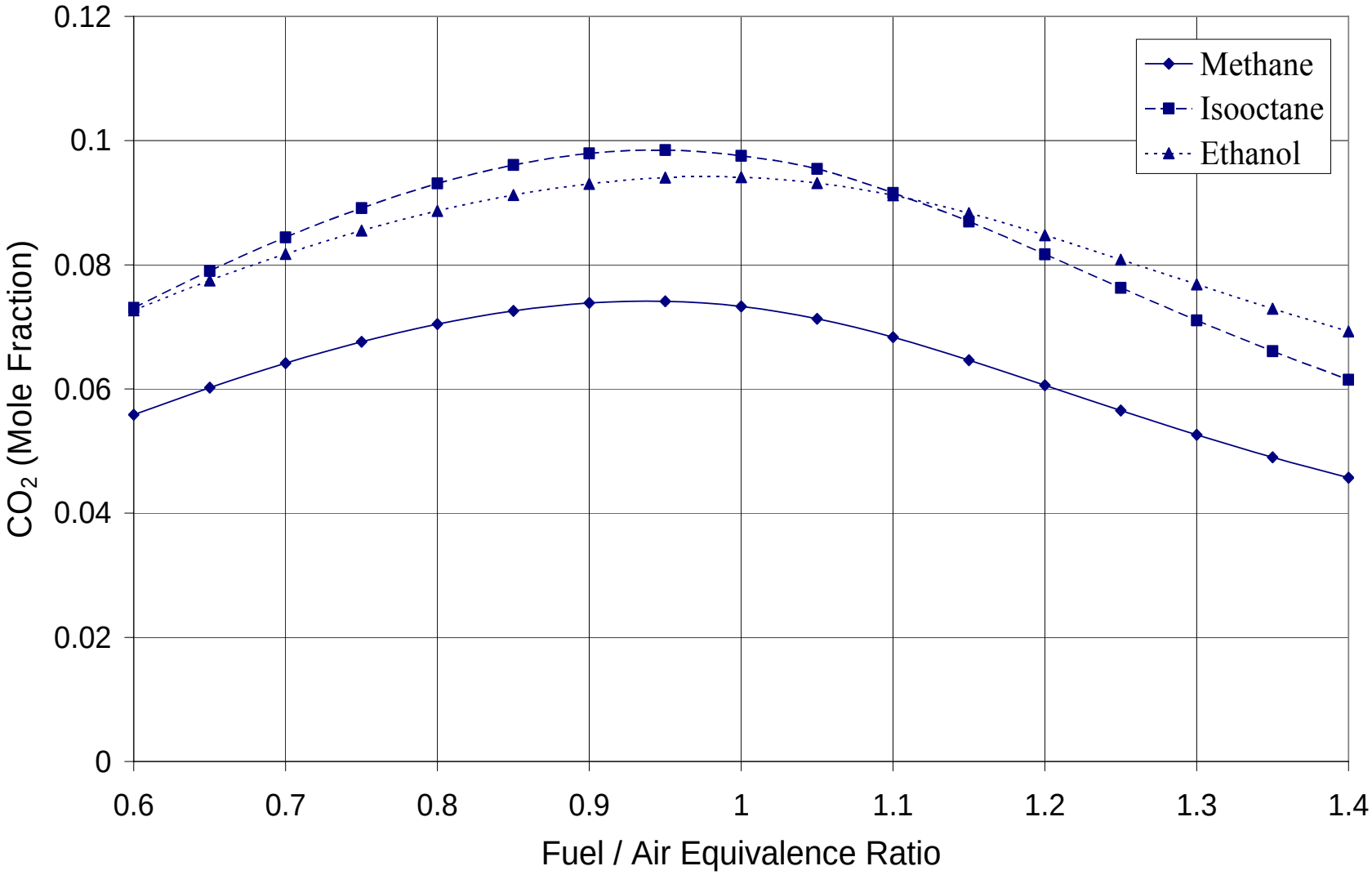

Figure 5.24: CO_2 Formation from the Combustion of Three Fuels in a PSR, p = 1 atm, τ = 5 ms

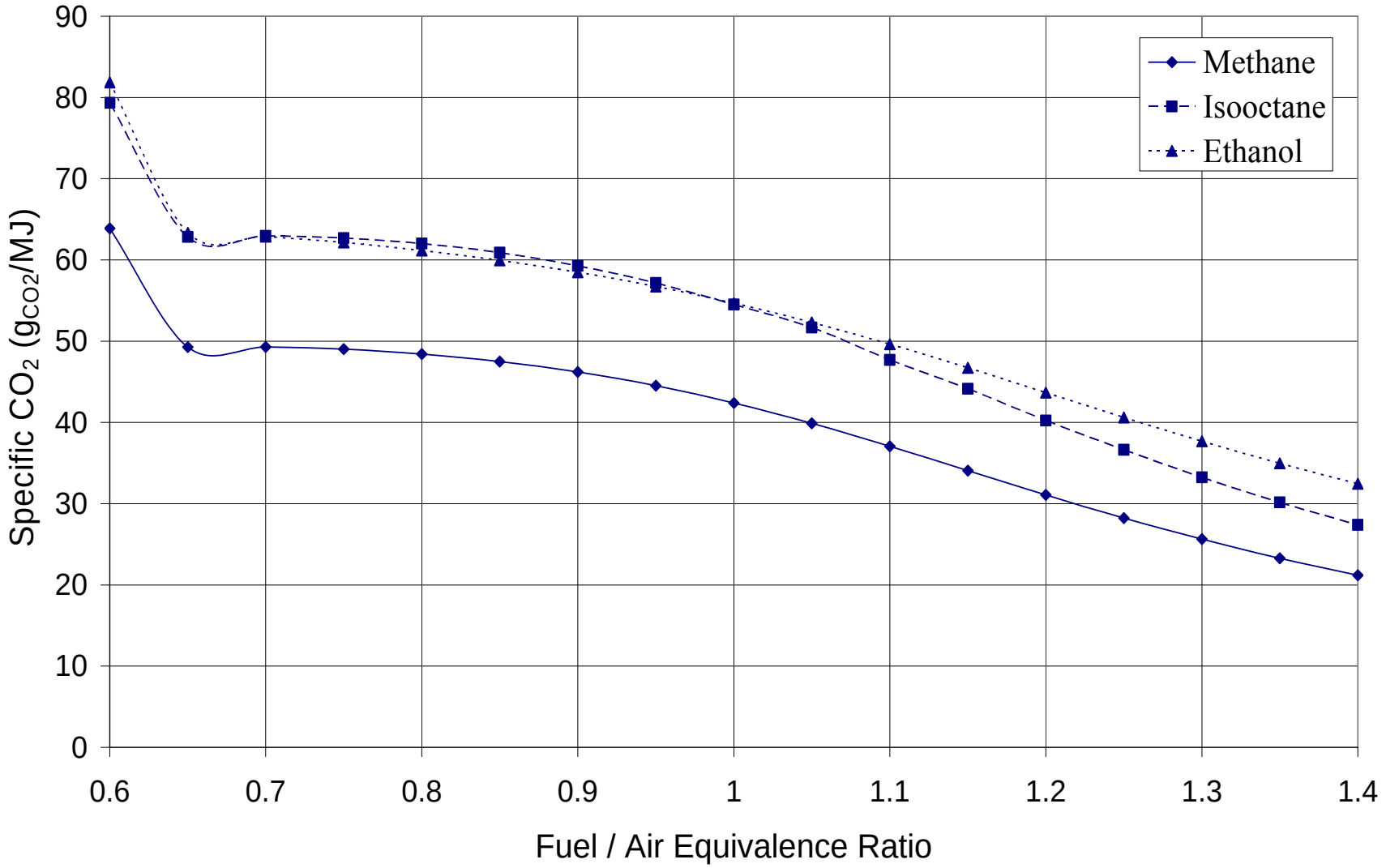

Figure 5.25: Specific Emissions of CO_2 from the Combustion of Three Fuels in a PSR, p = 1 atm, τ = 5 ms

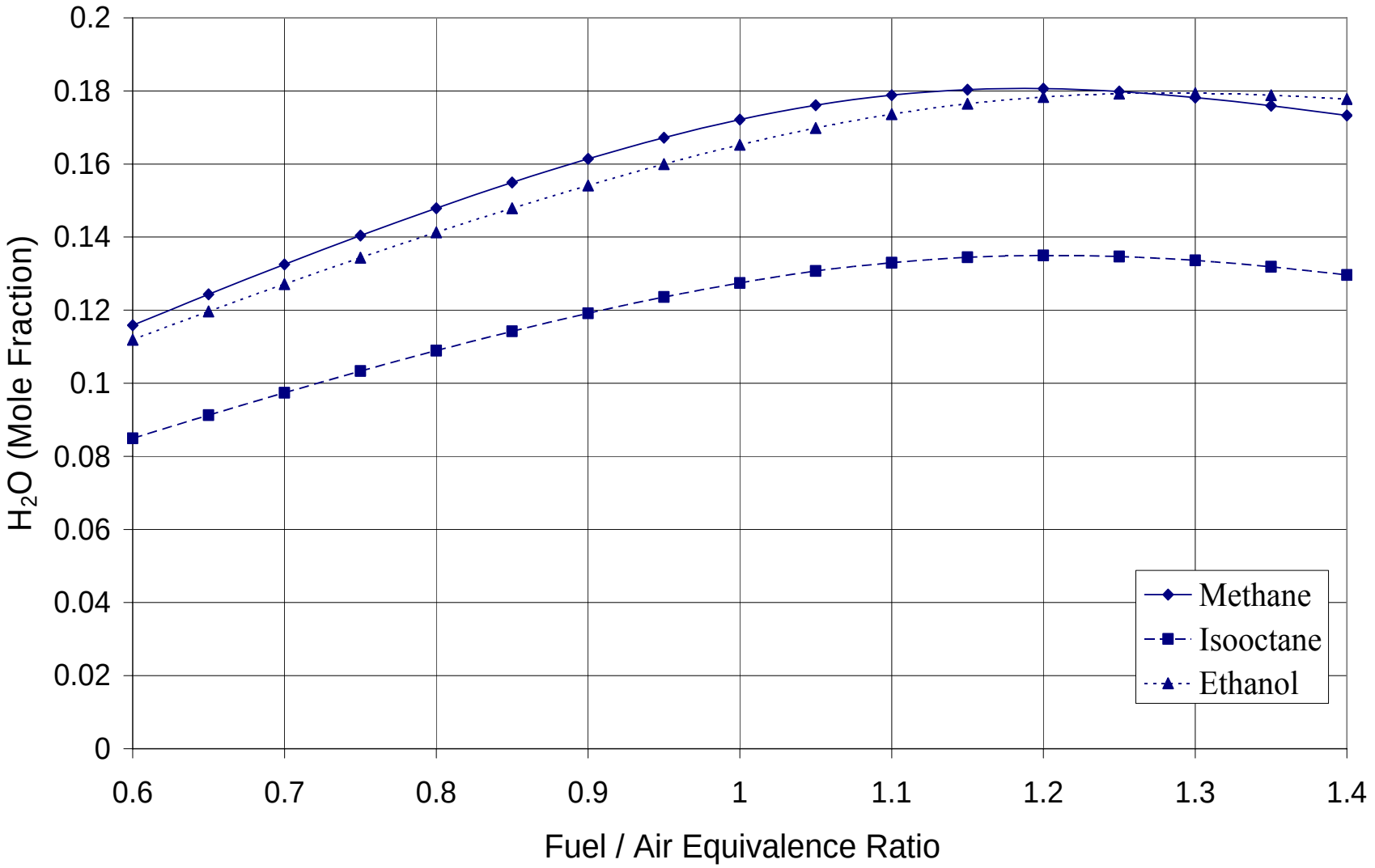

Figure 5.26: H_2O Formation from the Combustion of Three Fuels in a PSR, p = 1 atm, τ = 5 ms

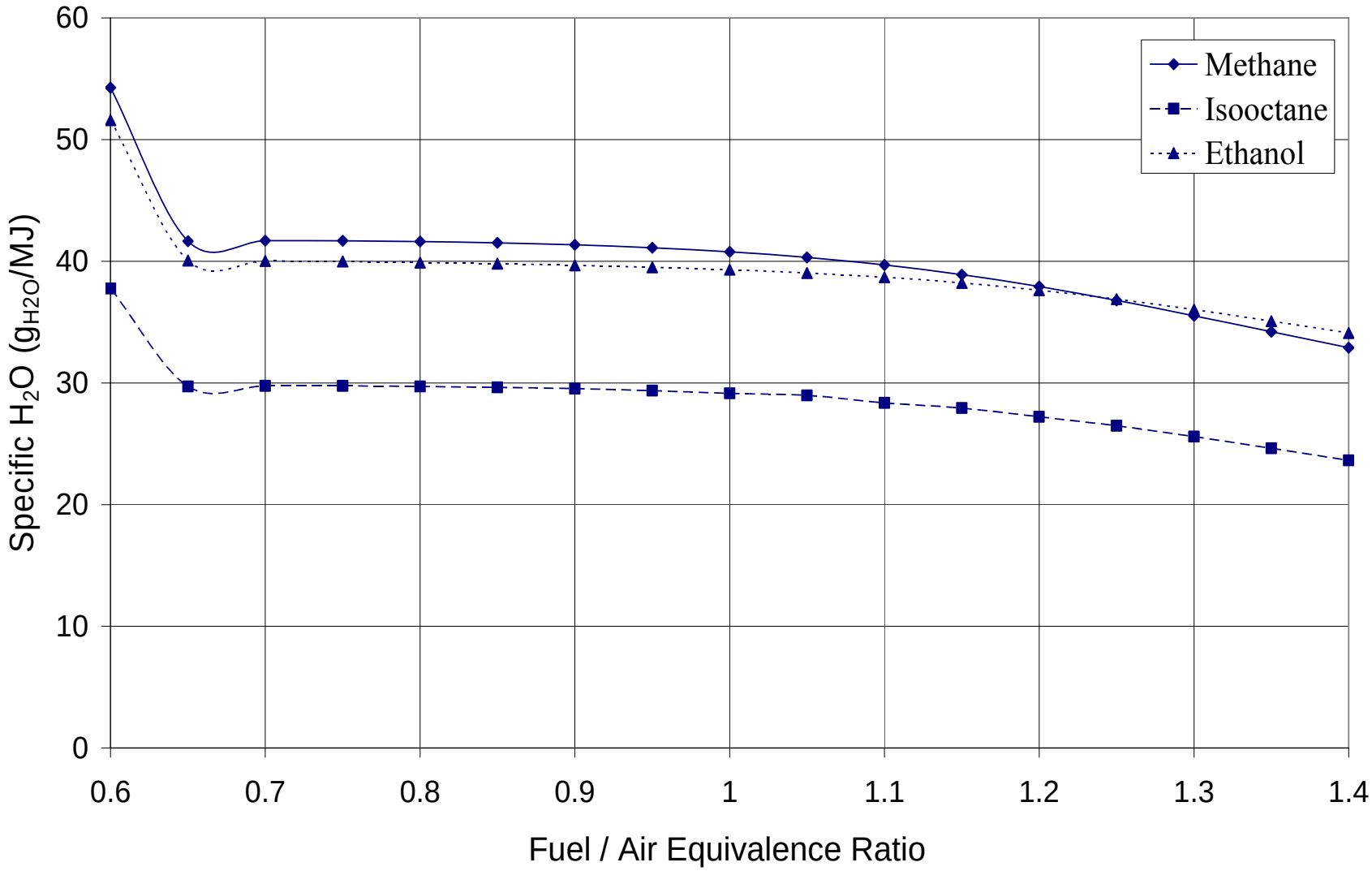

Figure 5.27: Specific Emissions of H_2O from the Combustion of Three Fuels in a PSR, p = 1 atm, τ = 5 ms

CHAPTER 6

CONCLUDING REMARKS

Combustion simulations of methane, isooctane, and ethanol with air in a perfectly stirred reactor have been performed using CHEMKIN (2006). The effect of changing the reactor pressure and charge residence time on adiabatic flame temperature and formation of pollutants CO and NO for methane and isooctane and CO for ethanol has been studied over a range fuel-air mixtures. A comparison of fuel flame temperatures and emissions has also been conducted. The emissions have been extended to include CO_2 and H_2O in the comparison section, where the formation is expressed in mole fractions as well as specific emissions where the mass produced is normalized by the fuel energy input.

Flame temperatures are observed to generally increase with reactor pressure and residence time for each fuel regardless of mixture strength. Peak temperatures are usually reached at slightly fuel-rich mixtures. This has been demonstrated to be due to the fact that the product of exiting mixture mass and specific heat is inversely proportional to the change in temperature. Isooctane is discovered to generate the highest temperatures followed by ethanol at equivalence ratios greater than 1.1 and methane at conditions lean of this point.

The CO formation increases as the mixture becomes fuel-rich and decreases with increasing pressure or residence time. These trends are exhibited by each fuel. High levels of

CO at rich conditions are explained by the lack of oxygen needed produce CO_2. Quantitatively, isooctane yields the highest CO at rich conditions while ethanol produces the highest at lean mixtures. Specific CO emissions are qualitatively similar to compositions represented in mole fractions for each fuel. It was reasoned that the fuel H/C ratio is the governing factor for CO emission levels.

NO formation for methane and isooctane combustion demonstrates its strong dependence on temperature. Peak NO typically is observed at mixtures generating the highest temperatures. The exception is for residence times of 1 ms where it has been suggested that the highly temperature dependent reactions of the extended Zeldovich mechanism are too slow to significantly contribute to overall levels in contrast to longer times of 5 and 10 ms. Peak values exist in the fuel-rich domain for 1 ms residence times and are significantly lower than for the longer times. To explain this, faster reactions significant to rich NO formation (prompt NO) discovered from previous studies are discussed. Isooctane produces larger NO than does methane due to its higher flame temperatures for all mixtures. Specific NO emissions are also larger for isooctane despite its higher molar energy content.

CO_2 formation is largest for isooctane at lean and slightly rich mixtures, whereas ethanol produces the highest levels for richer conditions. For each fuel, the lowest CO_2 levels are generated at the richest mixture considered. This is supported by the fact that CO to CO_2 conversion is limited in this domain. Specific CO_2 is very similar for isooctane and ethanol, and is essentially the same at stoichiometric mixtures. The combustion of methane yields the lowest mole fraction and specific CO_2 regardless of mixture strength.

The formation of mole fraction and specific H_2O is similar for methane and ethanol. The combustion of isooctane yields the lowest levels for all mixtures. This is attributed to the fuel H/C ratio being the primary determinant of H_2O emissions.

A number of fuels have been proposed to support the energy needs of the automobile and other combustion devices. This study has examined only three. There are many claims to the advantages of these various fuels; however, they must be treated with caution until supported by research. Computer simulation is an effective means of studying combustion performance, but it requires the development of complex kinetic mechanisms to describe the chemistry. Significant research and kinetic model refinement has been conducted on some fuels, such as methane, and therefore the mechanisms are considered accurate. However, many kinetic models are still in the developmental stages and the important aspects of H/C/N/O interaction remain to be uncovered. Work of this type is necessary before judgments can be made regarding the value of such fuels.

APPENDIX A

Table A.1: Specific CO Emissions.

	Specific CO (g/MJ)		
ϕ	Methane	Isooctane	Ethanol
0.60	2.25	2.55	3.09
0.65	1.73	1.94	2.77
0.70	1.91	2.12	3.29
0.75	2.27	2.53	3.95
0.80	2.81	3.19	4.74
0.85	3.56	4.12	5.68
0.90	4.54	5.37	6.78
0.95	5.79	6.94	8.06
1.00	7.31	8.85	9.54
1.05	9.09	11.04	11.24
1.10	11.07	13.49	13.13
1.15	13.13	16.11	15.18
1.20	15.15	18.66	17.29
1.25	17.03	21.11	19.36
1.30	18.73	23.34	21.31
1.35	20.22	25.34	23.09
1.40	21.48	27.10	24.69

Table A.2: Specific NO Emissions.

	Specific NO (g/MJ)	
ϕ	Methane	Isooctane
0.60	1.96×10^{-3}	6.43×10^{-3}
0.65	3.11×10^{-3}	9.48×10^{-3}
0.70	6.15×10^{-3}	1.80×10^{-2}
0.75	1.15×10^{-2}	3.41×10^{-2}
0.80	2.00×10^{-2}	6.01×10^{-2}
0.85	3.16×10^{-2}	9.40×10^{-2}
0.90	4.51×10^{-2}	1.28×10^{-1}
0.95	5.73×10^{-2}	1.55×10^{-1}
1.00	6.47×10^{-2}	1.69×10^{-1}
1.05	6.58×10^{-2}	1.64×10^{-1}
1.10	6.21×10^{-2}	1.57×10^{-1}
1.15	5.68×10^{-2}	1.41×10^{-1}
1.20	5.20×10^{-2}	1.24×10^{-1}
1.25	4.77×10^{-2}	1.07×10^{-1}
1.30	4.25×10^{-2}	9.14×10^{-2}
1.35	3.59×10^{-2}	7.70×10^{-2}
1.40	2.77×10^{-2}	6.42×10^{-2}

Table A.3: Specific CO_2 Emissions.

	Specific CO_2 (g/MJ)		
ϕ	Methane	Isooctane	Ethanol
0.60	63.90	79.34	81.86
0.65	49.27	62.82	63.36
0.70	49.29	62.97	62.88
0.75	49.02	62.71	62.15
0.80	48.43	62.02	61.18
0.85	47.51	60.90	59.96
0.90	46.21	59.29	58.49
0.95	44.52	57.16	56.74
1.00	42.40	54.51	54.69
1.05	39.88	51.67	52.32
1.10	37.05	47.70	49.64
1.15	34.06	44.14	46.73
1.20	31.07	40.23	43.67
1.25	28.23	36.64	40.63
1.30	25.63	33.24	37.70
1.35	23.28	30.15	34.96
1.40	21.18	27.38	32.45

Table A.4: Specific H_2O Emissions.

	Specific H_2O (g/MJ)		
ϕ	Methane	Isooctane	Ethanol
0.60	54.27	37.77	51.60
0.65	41.65	29.71	40.06
0.70	41.70	29.75	40.04
0.75	41.69	29.75	39.98
0.80	41.63	29.72	39.90
0.85	41.52	29.64	39.80
0.90	41.35	29.53	39.67
0.95	41.11	29.37	39.51
1.00	40.78	29.15	39.31
1.05	40.32	28.98	39.04
1.10	39.70	28.36	38.69
1.15	38.90	27.95	38.22
1.20	37.92	27.22	37.62
1.25	36.78	26.48	36.88
1.30	35.53	25.59	36.03
1.35	34.21	24.64	35.09
1.40	32.90	23.63	34.10

REFERENCES

Benson, S., 1976, "Thermochemical Kinetics," Wiley, NY.

Burcat, A. and McBride, B., 1993, "1994 Ideal Gas Thermodynamic Data for Combustion and Air- Pollution Use," Technical Report TAE 697.

CHEMKIN Release 4.1, 2006, Reaction Design, San Diego, CA.

Cohen, N. and Benson, S., 1993, *Chem. Rev.* **93**, 2419.

Dryer, F. and Glassman, I., 1978, *Prog. Astronaut. Aeronaut.* **62**.

Fenimore, C., 1971, "Formation of Nitric Oxide in Premixed Hydrocarbon Flames," *13th Symposium (International) on Combustion*, p. 373, Combustion Inst., Pittsburgh, Pennsylvania.

Fristrom, R. and Westenberg, A., 1965, "Flame Structure," McGraw-Hill, NY.

Giang, C., 2002, "Modeling of Hydrocarbon-Air Combustion and Emissions in a Perfectly Stirred Reactor," *M.S. Thesis*, The Ohio State University.

Giang, C. and Selamet, A., 2002, "Modeling of Nitrogen Oxide Formation from Isooctane-Air Combustion in a Perfectly Stirred Reactor," *AIAA* 2002-3711.

Glarborg, P., Miller, J., and Kee, R., 1986, "Kinetic Modeling and Sensitivity Analysis of Nitrogen Oxide Formation in Well-Stirred Reactors," *Combustion and Flame* **65**, 177-202.

Glassman, I., 1996, "Combustion," Third Ed., Academic Press, CA.

Hayhurst, A. and Vance, I., 1983, *Combustion and Flame* **50**, 41.

Heywood, J., 1988, "Internal Combustion Engine Fundamentals," McGraw-Hill, NY.

Himmelblau, D., 1974, "Basic Principles and Calculations in Chemical Kinetics," Prentice Hall, NJ.

Kee, R., Rupley, F., and Miller, J., 1987, "The Chemkin Thermodynamic Data Base," *Sandia National Laboratories*, Report SAND87-8215B.

Marinov, N., 1999, "A Detailed Chemical Kinetic Model for High Temperature Ethanol Oxidation," *International Journal of Chemical Kinetics* **31**, 183-220.

Maurice, L., 1996, "Detailed Chemical Kinetic Models for Aviation Fuels," *Ph. D. Thesis*, University of London.

McBride, B., 1991, "PAC91 Properties and Coefficients," *NASA Reference Publication 1271*.

Miller, J. and Bowman, C., 1989, "Mechanism and Modeling of Nitrogen Chemistry in Combustion," *Progress in Energy and Combustion Science* **15**, 287-338.

NIST Chemistry WebBook, 2005, http://webbook.nist.gov/chemistry/, Standard Reference Database 69, U.S. Secretary of Commerce.

Reid, R., Prausnitz, J., and Poling, B., 1987, "The Properties of Gases and Liquids," McGraw-Hill, NY.

Ritter, E. and Bozzelli, J., 1991, *International Journal of Chemical Kinetics* **23**, 767-778.

Turns, S., 1996, "An Introduction to Combustion: Concepts and Applications," McGraw-Hill, NY.